Received: 30 January 2019 | Revised: 4 May 2021 | Accepted: 14 May 2021

DOI: 10.1111/ejn.15314

RESEARCH REPORT

EJN European Journal of Neuroscience FENS WILEY

Modality-specific frequency band activity during neural entrainment to auditory and visual rhythms

Daniel C. Comstock[1] | **Jessica M. Ross**[2,3] | **Ramesh Balasubramaniam**[1]

[1]Cognitive and Information Sciences, University of California, Merced, CA, USA

[2]Berenson-Allen Center for Noninvasive Brain Stimulation, Beth Israel Deaconess Medical Center, Boston, MA, USA

[3]Department of Neurology, Harvard Medical School, Boston, MA, USA

Correspondence
Daniel C. Comstock, Sensorimotor Neuroscience Laboratory, Cognitive & Information Sciences, University of California, Merced, 5200 N Lake Road, Merced, CA 95343, USA.
Email: dcomstock@ucmerced.edu

Funding information
Division of Behavioral and Cognitive Sciences, Grant/Award Number: 1626505

Edited by: John Foxe

Abstract

Rhythm perception depends on the ability to predict the onset of rhythmic events. Previous studies indicate beta band modulation is involved in predicting the onset of auditory rhythmic events (Fujioka et al., 2009, 2012; Snyder & Large, 2005). We sought to determine if similar processes are recruited for prediction of visual rhythms by investigating whether beta band activity plays a role in a modality-dependent manner for rhythm perception. We looked at electroencephalography time–frequency neural correlates of prediction using an omission paradigm with auditory and visual rhythms. By using omissions, we can separate out predictive timing activity from stimulus-driven activity. We hypothesized that there would be modality-independent markers of rhythm prediction in induced beta band oscillatory activity, and our results support this hypothesis. We find induced and evoked predictive timing in both auditory and visual modalities. Additionally, we performed an exploratory-independent components-based spatial clustering analysis, and describe all resulting clusters. This analysis reveals that there may be overlapping networks of predictive beta activity based on common activation in the parietal and right frontal regions, auditory-specific predictive beta in bilateral sensorimotor regions, and visually specific predictive beta in midline central, and bilateral temporal/parietal regions. This analysis also shows evoked predictive beta activity in the left sensorimotor region specific to auditory rhythms and implicates modality-dependent networks for auditory and visual rhythm perception.

KEYWORDS

EEG, independent component analysis, neural oscillations, rhythm perception, time–frequency analysis

Abbreviations: ASR, artifact source reconstruction; cm, centimeters; Db, decibel; EEG, electroencephalography; ECoG, electrocorticography; ERSP, event-related spectral perturbation; Hz, hertz; ICA, independent component analysis; IOI, interonset interval; ITC, intertrial coherence; MAD, mean absolute deviation; MEG, magnetoencephalography; MRI, magnetic resonance imaging; ms, milliseconds; *SD*, standard deviation; SMA, supplementary motor area; SMS, sensorimotor synchronization; STS, superior temporal sulcus.

1 | INTRODUCTION

Perceiving a rhythm requires making predictions about the temporal onset of rhythmic events. This ability allows us to dance in time with music, play music with others, detect a musical beat, and notice when timing is off the beat. Common measures of rhythm perception are sensorimotor synchronization (SMS) tasks that involve synchronizing one's movements to rhythmic stimuli. Although most humans have little trouble synchronizing to auditory rhythms accurately, synchronizing to visual rhythms can be more variable. SMS to auditory rhythms are more reliable and adaptive (Chen et al., 2002; Lorås et al., 2012; Repp, 2003; Repp & Penel, 2004), compared with visual flashing rhythms (Comstock & Balasubramaniam, 2018; Repp & Su, 2013). However, when synchronizing movements with rhythmically moving visual stimuli such as a bouncing ball, synchronization accuracy improves, yet not to the level of auditory synchronization (Gan et al., 2015; Hove, Iversen, et al., 2013; Hove et al., 2010; Iversen et al., 2015). The reasons for the disparity in SMS accuracy across auditory and visual modalities are as of yet unclear, and a closer investigation of these mechanisms is required for a complete understanding of neural timing and synchronization processes. The present study aims to explore neurophysiological mechanisms of auditory and visual entrainment, particularly with regard to prediction of rhythmic events.

Previous functional magnetic resonance imaging (fMRI) research has shown there is overlap in the structures involved between visual and auditory rhythm perception, particularly within the premotor cortex, putamen, and cerebellum (Araneda et al., 2017; Hove, Fairhurst, et al., 2013). Although these areas appear to play a supramodal role in rhythm perception, putamen activation is stronger for auditory rhythms than for visual rhythms, suggesting the auditory system may be more tightly connected to timing networks (Araneda et al., 2017; Hove, Fairhurst, et al., 2013). There is also evidence from fMRI research suggesting the visual system has its own in-house rhythm timing mechanisms with sources in the parietal lobes (Jäncke et al., 2000; Jantzen et al., 2005), and in MT/V5 (Jantzen et al., 2005). The visual cortex has also been implicated in visual rhythm timing through ERP work (Comstock & Balasubramaniam, 2018) and through psychophysics work (Zhou et al., 2014). Taken together, we interpret this literature as support for modality-dependent rhythmic processing mechanisms, although to our knowledge this has not yet been clearly shown with a targeted electroencephalography (EEG) study.

Beyond modality-dependent rhythm processing, it has been suggested that neural timing mechanisms are task specific (Comstock et al., 2018; Wiener & Kanai, 2016). Evidence suggesting distinct aspects of rhythm timing and duration perception has been seen in the cerebellum through lesion work (Grube et al., 2010), and work using transcranial magnetic stimulation (TMS) (Grube et al., 2010), additional evidence is seen through TMS work involving the posterior parietal lobes (Ross et al., 2018) suggesting a specific role for duration timing in the cerebellum, whereas the posterior parietal cortex is involved in rhythm timing. Much of the evidence supporting predictive processing for rhythm comes through measures of neural oscillation within different frequency bands. This oscillatory modulation is believed to indicate communication between different regions of the brain, with lower frequency oscillations involved more in communication between regions that are farther away from each other, and higher frequencies involved more in localized communication (Sarnthein et al., 1998; Von Stein & Sarnthein, 2000). Furthermore, Bastos et al. (2015) have shown in non-human primates using electrocorticography (ECoG) that activity in the gamma and theta bands are involved in feedforward, or bottom-up visual processing, whereas the beta band is involved in feedback, or top-down visual processing. Michalareas et al. (2016) have shown similar results in human visual cortical areas with gamma involved in bottom-up processing and alpha and beta involved in top-down processing by correlating human magnetoencephalography (MEG) data with corresponding macaque neural anatomy. Interestingly, Michalareas et al. (2016) also found that alpha and beta top-down processing affects the ventral and dorsal visual stream areas differently, by shifting dorsal stream activity higher in the functional hierarchy of visual processing, whereas ventral stream downward. If frequency band activity relates to specific top-down or bottom-up processing networks, then by measuring frequency band activity during different rhythm timing tasks we can find markers of the networks involved, supporting different networks for different tasks. Neural oscillations within different frequency bands are therefore a rich source of information for investigating timing networks.

Neural mechanisms of auditory rhythm perception have been suggested to rely on strong interactions between motor systems and auditory cortices (Iversen & Balasubramaniam, 2016; Janata et al., 2012; Repp & Su, 2013; Ross, Iversen, et al., 2016; Ross, Warlaumont, et al., 2016), possibly mediated through projections in parietal cortex (Patel & Iversen, 2014; Ross et al., 2018). Communication across these networks could be carried out through frequency band-specific oscillatory activity. Activity in the beta band (14–30 Hz) is of primary interest as it has been shown to play a role in prediction and timing for auditory rhythms using EEG (Snyder & Large, 2005) and MEG (Fujioka et al., 2009, 2012, 2015), as well as being implicated in the onset of movements (Kilavik et al., 2013).

Snyder and Large (2005) found differentiation between induced and evoked activity in EEG high beta and low gamma bands (20–60 Hz), where induced activity was defined as not phase locked to a stimulus onset and evoked activity was

defined as phase locked to the stimulus onset. By presenting subjects with a sequence of tones with occasional tones omitted, Snyder and Large found induced activity was similar in tone trials and omitted tone trials, indicating expectation for the tones in the sequence, whereas evoked activity was greatly reduced when there was no tone. Fujioka et al. (2009) used a similar omission paradigm with MEG and found induced beta from auditory cortices decreased after tone onset and increased in anticipation of the expected tone onset. A later MEG study showed the rate of beta increase in anticipation of tone onset is dependent on the tempo of the stimulus, whereas beta decrease following tone onset is consistent across multiple tempi (Fujioka et al., 2012). Fujioka et al. (2012) additionally found cortico-cortical coherence that followed the tempo of the rhythms between auditory cortices and sensorimotor cortex, supplementary motor area (SMA), inferior-frontal gyrus, and cerebellum.

The role of beta activity in visual rhythm perception is less studied. However, beta band amplitude modulation arising from the motor cortex has also been implicated in visually mediated temporal cues indicating expectation in a study using an implanted multielectrode array in the primary motor cortex (Saleh et al., 2010). More recently, Varlet et al. (2020), showed cortico-muscular coupling of beta-band activity induced by audio-visual rhythms between EEG recorded over motor areas and EMG recorded from finger muscles pressing down on a force sensor. Significantly, the coupling appeared to be modulated by the tempo of the rhythm and peaked roughly 100 ms prior to each tone in the sequence. Interestingly, the study did not find significant cortico-muscular coupling in response to separate auditory or separate visual rhythms. Although Saleh et al. (2010) and Varlet et al. (2020) suggest involvement of beta band modulation in visual rhythm perception, the role of beta band activity in visual rhythm perception remains unclear.

To investigate predictive mechanisms of rhythm perception across modalities, we used EEG to record beta band modulation during auditory and visual rhythms. To separate out the stimulus response activity from activity related to temporal prediction of the stimulus we used an omission paradigm similar to that used by Snyder and Large (2005) and Fujioka et al. (2009). Given that previous studies have indicated involvement of sensory and motor-related beta in rhythm perception (Fujioka et al., 2012, 2015; Varlet et al., 2020) we describe all Beta band activity. Because EEG activity smears at the scalp it can be difficult to separate out concurrent sources of activity. We used independent component analysis (ICA) as a blind source separation method in an attempt to distinguish sensory and motor related activity.

Based on the assumption that beta oscillations play a general role in top-down processing, we hypothesized that we would find induced beta power modulation for both auditory and visual modalities following the same pattern seen in Fujioka et al. (2009). Specifically, we hypothesized we would find an induced increase in beta in anticipation of the onset of each rhythmic stimulus event, and also prior to the expected onset of an omitted event (omission onset), followed by a sharp decrease in beta power after event onset, but not after omission onset. Furthermore, we expected that evoked beta power would increase only in response to stimulus onset and not in anticipation of omission onset based on the findings of Snyder and Large (2005). Because the motor system has been implicated in both auditory and visual rhythm perception, and evidence of motor related beta for rhythm perception has been seen for auditory rhythms (Fujioka et al., 2012, 2015), and implicated in visual rhythms (Varlet et al., 2020), we expected to find motor related predictive beta activity for both auditory and visual modalities. To explore modality-specific characteristics of predictive beta without prior assumptions about visual and auditory mechanism or network contributions to predictive beta, we performed an exploratory ICA-based clustering technique using component spatial information (dipole locations and scalp topographies) to group similar sources that were shared across subjects. To avoid bias in cluster interpretation, we present and describe in detail all clusters.

2 | MATERIALS AND METHODS

2.1 | Participants

A total of 18 subjects participated in the experiment (11 female, average age of 23.6 (20–34)) with one being rejected after data collection for poor signal to noise ratio. All participants were right-handed and had typical hearing and typical or corrected vision. The experimental protocol was carried out in accordance with the Declaration of Helsinki. This study was approved by the UC Merced Institutional Review Board for research ethics and human subjects, and all participants gave informed consent prior to testing.

2.2 | Task

After subjects gave written consent, they were seated and fitted with a 32 electrode EEG cap. Subjects were then tasked with watching isochronous flashing visual rhythms or listening to isochronous auditory rhythms. Both kinds of rhythms had an interonset interval (IOI) of 600 ms, and both had occasional omissions of single tones or single flashes. The rhythms were broken into stimulus trains with each train consisting of 100 tones or flashes with 7 omitted tones or flashes placed randomly within the train. The location of the omitted tones or flashes in the stimulus trains were constrained such that there must be at least 8 tones or flashes between each

omission. There were 20 stimulus trains per condition for a total of 140 omissions in each condition. Subjects completed all of the stimulus trains in one modality, followed by all of the stimulus trains in the other modality, in design counterbalanced across subjects. Before the omission conditions, subjects were presented with a condition with no omissions consisting of 140 tones or flashes. The non-omission stimulus trains were of the same modality as the omission stimulus trains that would follow. This design resulted in 140 trials for each of the four conditions (tone non-omission, tone omission, flash non-omission, flash omission; Figure 1).

To ensure that subjects were attending to the rhythms, after each train a shorter sequence of 5 tones or flashes was presented at a slightly slower or faster tempo than the experimental train, and subjects were asked to determine if the shorter rhythm was slower or faster than the preceding rhythm. The number of correct responses and response times were recorded and used to determine if subjects were adequately attending to the stimulus trains.

The auditory metronome consisted of 1,000 Hz tones lasting 50 ms with a 10 ms rise and 40 ms fall time, generated using Audacity digital audio software. The visual metronome consisted of light gray square flashes 3 × 3 cm lasting 50 ms each. In both cases, there was a black screen with a dark gray fixation cross in the center of the screen where the lines were approximately 3 mm wide and 4 cm long. The visual flashes always appeared behind the fixation cross so that the cross never disappeared when the flash appeared behind it.

The stimuli were presented using Paradigm experimental stimulus presentation software (Perception Research Systems, 2007) on a 60 Hz monitor, which was approximately 65 cm from the subject's head. Subjects responded to any prompts using a keyboard placed on a desk in front of the chair they were seated in.

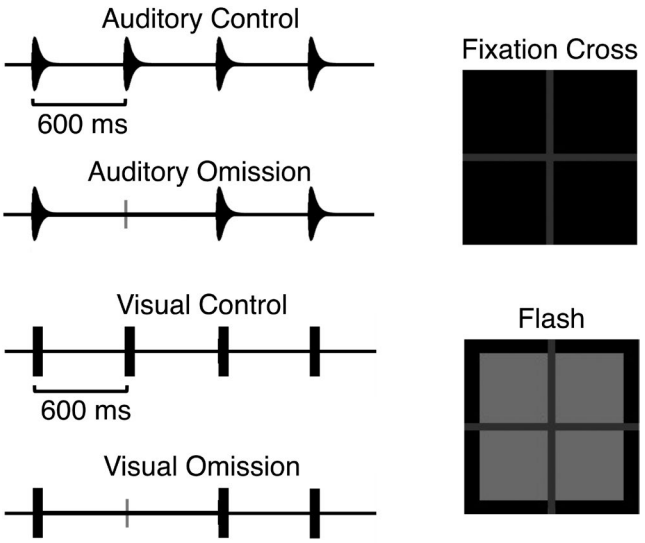

FIGURE 1 Schematic of control and omission conditions for both auditory and visual metronomes, and depiction of the visual flash metronome stimuli. The fixation cross was always visible for both auditory and visual conditions, even when the flash appeared in the visual condition

2.3 | EEG data acquisition and processing

Electroencephalography was continuously recorded using an ANT-Neuro 32 channel amplifier with the ANT-Neuro 32 electrode Waveguard cap. The electrodes were situated according to the 10–20 International system and EEG was recorded with a sampling rate of 1,024 Hz. The data were then processed using the EEGLAB v14.1.1 toolbox (Delorme & Makeig, 2004) within MATLAB 2019. Channel locations were added using the standard location montage for the Wavegaurd cap. EEG data were first pruned by hand to remove sections between stimulus train blocks. This was done to remove any break periods between trains. Following pruning, the data were down-sampled to 256 Hz and then a high-pass filter with a 2 Hz passband edge and 6 dB cutoff at 1 Hz was applied. A low-pass filter with a 50 Hz passband edge and 6 dB cutoff at 56.25 Hz was applied to remove 60 Hz line noise. Bad channels were rejected that had activity with lower than 0.8 correlation with their surrounding channels with the maximum channels rejected for any one subject being 5 ($M = 2.71$, MAD = 1.31). Rejected channels were then interpolated using spherical interpolation. We then removed single-channel artifacts using artifact source reconstruction (ASR), which has been shown to effectively remove large-amplitude or transient artifacts in the data (Chang et al., 2018; Mullen et al., 2015). ASR was performed using a conservative burst criterion parameter of 50 *SD*s. After ASR was run, we then re-referenced the data to average. To separate out non-brain artifacts and for the source-level analysis, we ran ICA using the AMICA ICA algorithm (Palmer et al., 2012). Dipole source localization was performed on the resulting components using the MNI head model, and two dipoles were fit where appropriate instead of one using the FitTwoDipoles plug in (Piazza et al., 2016). ICA components were checked to find eye blink and cardiac components, which were marked for later rejection. The remaining independent components were used for source analysis.

We then segmented the continuous data into four long epochs for the experimental conditions: Non-omission visual flashes, non-omission auditory tones, visual omissions, and auditory omissions. The non-omission conditions came from the non-omission stimulus train block that preceded the omission block. Each condition was epoched from −1.67 s prior to each tone/flash to 1.67 s following the tone/flash. Epoch length was determined by calculating the window size needed for the later time/frequency calculations, so the resulting time/frequency data would span ±1.5 s from the tone

or flash onset of interest. The omission groups were epoched in the same way in relation to omission events. Following epoching, epochs were checked for blinks that occurred during either event onset (for the non-omission conditions) or expected onset (for the omission conditions) as defined as a 50 μV or larger spike in frontal electrodes within ±100 ms of onset or expected onset. After epochs with eye blinks at event onset, or expected onset, were rejected, eye blink components determined by AMICA marked earlier were then rejected. Remaining epochs with amplitude spikes greater than ±500 μV were then rejected. Finally, epochs that were deemed improbable were rejected by computing the probability distribution of values across the epochs for individual channels and across all channels. Any epoch that contains data values >6 *SD*s for the channel or 2 *SD*s for all electrodes was rejected. One subject was rejected due to having more than 50% of their total epochs being rejected. For the remaining 17 subjects there were 140 possible epochs per condition per subject for the four conditions: visual non-omission ($M = 123.24$, max = 136, min = 96, MAD = 13.27), visual omission ($M = 116.59$, max = 132, min = 74, MAD = 18.19), auditory non-omission ($M = 118.29$, max = 136, min = 92, MAD = 14.24), auditory omission ($M = 109.06$, max = 129, min = 66, MAD = 20.12).

2.4 | Clustering procedure

Electroencephalography activity measured at the electrode level is smeared across the scalp making it difficult to separate out signals from different sources. Because we are interested in time-sensitive neural activity from both sensory and motor areas that occur simultaneously, we focus our analysis on the source-level activity of components. To compare independent components across subjects, we performed a cluster analysis using *k*-means clustering based on the component dipole locations and component scalp topographies using EEGLAB's clustering tools (Delorme & Makeig, 2004). Using both dipole locations and scalp topographies allows for clusters that are more consistent across subjects than can be computed using a single measure (Onton et al., 2006). This clustering approach avoids statistical double dipping by excluding the measures of interest (event-related spectral perturbation [ERSP] and intertrial coherence [ITC]), and focusing only on the spatial features of the components. Dipole location and scalp topography were weighted equally, and PCA was applied to the component scalp topography data reducing the number of dimensions to 3, matching the number of dimensions in the dipole locations and therefore reducing the overall number of dimensions to cluster. To ensure non-brain sources, including muscle activity and channel noise, were excluded from clustering, only components with dipoles located within the head and with a residual variance of less than 15% were used resulting in a total of 289 total brain components across 17 subjects. The group of all 289 components prior to clustering constitute the parent cluster, which we used to look at global-level activity. To determine the appropriate number of clusters, we applied three measures for cluster number optimization (Calinski-Harabasz, Silhouette, and Davies-Bouldin) for between 5 and 30 clusters. The Calinski-Harabasz and Silhouette methods indicated the optimal number of clusters was 9, whereas the Davies–Bouldin method indicated an optimum number of 13. We used nine clusters to maximize the number of unique subjects per cluster, plus one outlier cluster with components with positions of more than 3 *SD*s from any of the cluster centers. The resulting nine clusters (Figure 2; Table 1) averaged 31.88 components per cluster with a standard deviation of 7.17, which were made up from 15.78 subjects on average, standard deviation 0.97. The outlier cluster consisted of three components from two subjects. No cluster had more than five components from any one subject. Table 1 shows the individual makeup of each cluster.

2.5 | Time–frequency analysis

Time–frequency analysis was completed for each subject at each channel and for each component used in the clustering analysis. The resulting time–frequency representations were then averaged across subjects for the individual channels in each condition and averaged across the components for each cluster for each condition. Induced and evoked time–frequency representations were calculated to determine the different roles they play during the rhythm perception task as they have been found to play different roles in auditory rhythm perception (Snyder & Large, 2005). Induced activity was calculated for each trial by first removing the mean of activity (ERP) from each trial so only non-phase locked activity remains, and then averaging the resulting time–frequency computations across trials. Evoked activity was calculated on the mean of the activity (ERP) to focus on the phase locked activity. All three time–frequency calculations were performed using the same parameters. The time–frequency calculations were computed with the *newtimef* function in EEGLAB (Delorme & Makeig, 2004) using 85 linear spaced Morlet wavelets between 8 and 50 Hz with a fixed window size of 300 ms resulting in 2.4 cycles at 8 Hz and scaling up to 15 cycles at 50 Hz. The 300 ms window size was chosen to ensure the time–frequency representation from each individual stimulus was not contaminated by either surrounding stimuli, which were 600 ms apart. The convolution used the minimum step size for the sample rate of 256 Hz resulting in 772 evenly spaced steps with a step length of 3.9 ms. Baselines were computed separately for each condition using a relative to the mean baseline with

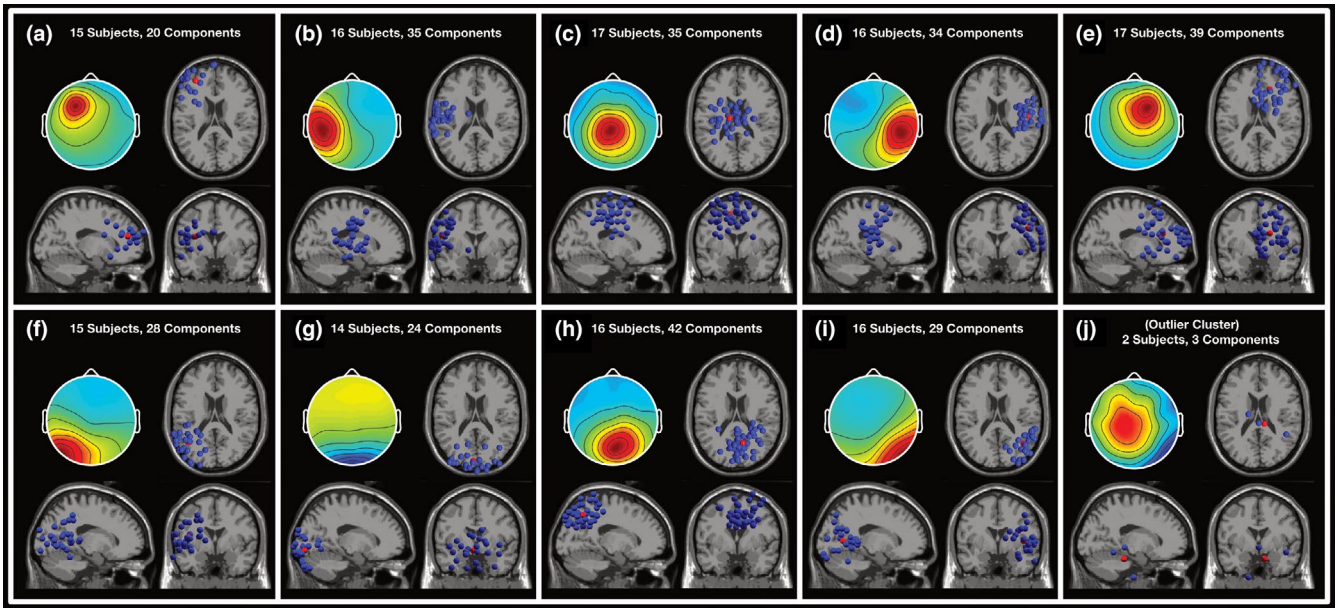

FIGURE 2 Scalp topography and dipole locations of components for the nine clusters and the outlier cluster. Scalp topography includes activity from all four conditions. Blue dots indicate individual component dipole locations. Red dots indicate the average position

a period of −1,200 to −600 ms from the stimulus or omitted stimulus onset, dependent on condition. This baseline period consisted of one complete 600 ms stimulus cycle for both the omission and control conditions, allowing us to focus on the oscillatory dynamics between stimulus events. Separate baselines for each condition were used to minimize effects of individual variation and of differences that might arise between omission and non-omission conditions due to habituation to stimuli in the unvarying and longer blocks in the non-omission conditions. Although a common baseline would allow us to determine overall power differences between conditions in the frequency bands, our focus is on the changes in power that occur within condition within the timeframe of each stimulus train as described later in the slope analyses description. These computations were used to determine the ERSP values in terms of dB, such that the ERSP plots show shift in power from baseline at each time point.

To ensure changes in evoked activity were due to stimulus-driven phase shifts, we additionally calculated phase coherence across trials using the ITC measure in the *newtimef* function of EEGLAB (Delorme & Makeig, 2004). ITC is calculated by extracting the phase angle at each time–frequency point for each trial and comparing the phase angles across trials for coherence providing a coherence measure between 1 and 0, where 1 indicates complete coherence across trials for a given time–frequency point, and 0 indicates no coherence across trials. The ITC calculation required an additional time–frequency computation of the data using the same parameters as was done for induced activity except there was no subtraction of the ERP.

Beta activity was extracted from the ERSP values by averaging the power at each step between 14 and 30 Hz. Beta ITC was extracted using the same procedure except applied to ITC values instead of ERSP values.

3 | ANALYSIS

3.1 | Attention behavioral task

To assess if attention was maintained evenly between the two modalities, we analyzed the behavioral data from the attention task for the two omission conditions. Both auditory (94.72%) and visual (88.61%) conditions showed a correct response rate well above chance. To assess the differences between the auditory and visual conditions, the number of correct responses and response times were assessed using paired *t* tests. There was a significant difference in number of correct attention trials between the auditory ($M = 18.94$, $SD = 1.09$) and visual ($M = 17.65$, $SD = 1.69$) conditions; $t(16) = -2.72$, $p = 0.015$ which we ascribe to the visual rhythm task being more difficult than the auditory rhythm task. There was no significant difference in response time measured in ms between auditory ($M = 1{,}405.04$, $SD = 572.09$) and visual ($M = 1{,}495.99$, $SD = 585.94$) conditions; $t(16) = 0.66$, $p = 0.52$.

3.2 | Event-related spectral perturbations

To determine if ERSP power was being significantly modulated by the stimuli and omissions, permutation statistics

TABLE 1 Information containing the component make-up of the nine clusters and outlier cluster. Although the corresponding Brodmann area for each cluster is determined based on the average Talaiarch coordinates of the component dipoles, the dipole locations for the individual components for each cluster are not all contained within the indicated Brodmann area. Individual dipoles for each component are shown in Figure 2. Components per subject column indicates both the average number of components per subject in the cluster, and the maximum components any single subject had in the cluster

Cluster	Subjects	Components	Components per subject	Mean R.V. %	Mean Tal coordinates	Corresponding Brodmann area of mean coordinates
1—Left frontal	15	20	Avg = 1.33 Max = 3	5.88	X: −31 Y: 45 Z: 14	Left area 10
2—Left sensorimotor	16	36	Avg = 2.19 Max = 4	5.86	X: −53 Y: −12 Z: 19	Left BA 1/4 (primary sensory/ primary motor)
3—Midline central	17	35	Avg = 2.06 Max = 3	6.54	X: −12 Y: −12 Z: 51	Left BA 6
4—Right sensorimotor	16	34	Avg = 2.13 Max = 4	5.21	X: 49 Y: −9 Z: 30	Right BA 4 (primary motor)
5—Right frontal	17	39	Avg = 2.29 Max = 4	7.07	X: 18 Y: 32 Z: 20	Right BA 8/9
6—Left temporal/parietal	15	28	Avg = 1.87 Max = 4	4.49	X: −42 Y: −58 Z: 13	Left BA 39 (angular gyrus)
7—Occipital	14	24	Avg = 1.71 Max = 3	4.52	X: −4 Y: −87 Z: −5	Left BA 18 (visual assoc)
8—Parietal	16	42	Avg = 2.63 Max = 5	4.42	X: 10 Y: −58 Z: 45	Right BA 7
9—Right temporal/parietal	16	29	Avg = 1.81 Max = 3	3.42	X: 41 Y: −61 Z: 7	Right BA 19/37 (peristriate area/ fusiform gyrus
10—(Outlier)	2	3	Avg = 1.5 Max = 2	7.03	X: 10 Y: −31 Z: −19	Null

comparing ERSP power values to baseline values using unpaired *t* tests with 2,000 permutations testing for significance were performed. False discovery rate (FDR) correction was used to correct for multiple comparisons with alpha values being the computed *p*-value for each time–frequency point using a parametric FDR algorithm (Benjamini & Hochberg, 1995).

3.3 | Beta band slope analysis

Although significance testing in ERSP power can indicate significant power modulations in response to stimuli, we are interested in the dynamics of beta band activity following findings that indicate beta power rises to peak at the expected onset of an auditory tone followed by a trough after a tone, where the rate of the rise beta power, yet not the fall, is dependent on the tempo of the stimuli (Fujioka et al., 2012). Since we hypothesized that rise in beta activity is related to the timing of the rhythmic stimuli, we would see beta power rise prior to the expected onset of the omitted stimuli at the same rate as beta would rise prior to the non-omitted stimuli. Furthermore, by investigating the slope of activity prior to the omission onset, we have a measure that is less likely to be affected by activity due to a response to the omission. To test this hypothesis, two slopes were fitted in the averaged beta activity for each subject for each condition based on a least squares measure in a procedure similar to that performed by Meijer et al. (2016). The first slope started at −300 ms prior to stimulus or omission onset and ended at stimulus or omission onset (0 ms). Using −300 ms as the starting point was chosen as the halfway point between stimuli. Because there is considerable variation across subjects in slope activity, a second slope was fitted starting at the lowest measured activity between −300 and −100 ms and ending at stimulus or omission onset. Although comparing the slopes of the omission and non-omission condition could tell us if the two slopes are significantly different, our goal is to show that the two slopes are not significantly different and in fact are very similar. One way to show this is to compare against a third condition. To provide the third condition for comparison, we shuffled the ERSP data used to find slopes in the control condition for each subject at each channel, and for each component for each cluster, and then extracted beta band power and fitted slopes. Fitting a slope to the beta band extracted from the shuffled ERSP power results in an effective slope of 0, which we use to compare the other slopes to. For the shuffled condition, ERSP power values along the entire time

axis of each epoch of each frequency step were randomly shuffled 1,000 times using the *randperm* function in Matlab. Beta band power for each time point was then extracted from resulting shuffled ERSPs, the same as done with the non-shuffled ERSPs. Slopes were then fitted in the same way as with the non-shuffled data, except that instead of finding the minimum beta power between −300 and −100 ms for the shuffled condition, we used the same starting point used in the non-shuffled control condition for the corresponding subject or component. Figure 3 depicts slope fitting to beta band from the trough to 0 ms.

Four sets of *t* tests were used to determine if the fitted slope of beta activity prior to the onset of a tone or flash was equivalent to the fitted slope of beta activity prior to the expected but omitted onset of a tone or flash for both induced and evoked activity and for both the slopes fitted from −300 ms to onset and for the slopes fitted to the trough between −300 and −100 ms and onset. FDR correction was used to correct for multiple comparisons for all *t* tests using the method described in Benjamini and Hochberg (1995) with alpha set to 0.05. The first three analyses were performed using paired *t* tests comparing: the slopes of the omission conditions to the slopes of the non-omission conditions, the slopes of the non-omission conditions to the slopes of the shuffled conditions, and the slopes of the omission conditions to the slopes of the shuffled conditions. If beta power is being modulated such that it shows anticipation of the stimulus we would expect both the omission and control fitted slopes to indicate beta power is rising prior to stimulus onset, and therefore be significantly different from the shuffled fitted slopes, which are effectively flat. Additionally, we would expect the omission and non-omission fitted slopes to not be significantly different from each other as they both rise in anticipation of the incoming event regardless if that event is omitted or not.

Showing that a fitted slope in the omission condition is not significantly different than a fitted slope in the non-omission condition, and that both omission and non-omission-fitted slopes are significantly different than the shuffled slopes is not sufficient to claim that the slopes in the omission and non-omission conditions are equivalent. This is because a comparison between significant results and non-significant results is not necessarily significant (Gelman and Stern, 2006), and therefore, an additional test is required. To assess the viability of the comparison between the two results, we applied a post hoc comparison test as used in Abbott and Shahin (2018). The test calculated if the slope of the non-omission condition + the slope of the shuffled condition – 2 × the slope of the omission condition was significantly different from zero using a *t* test with the same FDR correction as used for the other *t* tests at each channel and each cluster. With these four tests, we show the beta slope is showing anticipation of the next event and that the slope of the omission condition is equivalent to the slope of the non-omission condition if: (a) the omission and non-omission slopes are not significantly different, (b) both the omission and non-omission slopes are significantly different from the shuffled (flat) slope, (c) the post hoc comparison test of the three slopes is significant showing omission and non-omission slopes are equivalent.

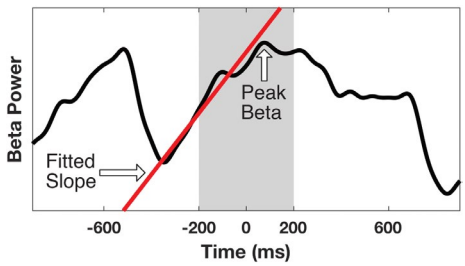

FIGURE 3 Schematic for slope fitting and peak finding for beta activity. Slopes were fitted between the trough (between −300 and −100 ms) and 0. Peak beta was determined between −200 and 200 ms (range depicted in shaded area). Slopes were fitted for evoked and induced beta power, whereas peaks were found in evoked and induced beta power as well as in intertrial coherence in the beta range

3.4 | Evoked and induced comparison

To further understand the different roles evoked and induced beta play in the temporal aspects of auditory and visual rhythm processing, we applied an additional exploratory analysis that measured peak power and peak time in response to both present and omitted tones and flashes similar to performed by Snyder and Large (2005). To make the comparison, ERSP power P was converted from dB to μV^2 and normalized using the formula: $P_{norm} = (P - P_{min})/(P_{max} - P_{min})$. This normalization conversion resulted in values between 0 and 1 and was applied to ERSP values for both evoked and induced activity for each individual component for each cluster, after which beta power was extracted in the same manner as done for the slope analyses. Peak power and peak time were determined by finding the time and normalized power of the peak power between ±200 ms of the expected event onset. Paired *t* tests were then run on each cluster as well as the parent cluster to determine the roles evoked and induced activity within each cluster. All *t* tests used FDR correction to account for multiple comparisons (Benjamini & Hochberg, 1995).

3.5 | Intertrial coherence

While measuring induced and evoked activity allow us to contrast our results to the work from Snyder and Large (2005), neither measure provides a direct measure of the

changes in phase coherence in relationship to the omission and non-omission onsets. We use ITC to confirm that the evoked activity we measure is due to phase coherence by comparing peak times of beta ITC with peak times of beta induced and evoked activity. The same procedure was used to extract beta coherence and find peaks as was used to find the peaks in induced and evoked beta activity. Paired *t* tests comparing ITC beta peak times with induced and evoked peak times were then run on each cluster including the parent cluster. All *t* tests used FDR correction to account for multiple comparisons (Benjamini & Hochberg, 1995).

3.6 | Baseline comparison

To assess potential differences in habituation to the stimuli, an analysis was performed on the computed baseline levels across non-omission and omission conditions within each modality. Although differences in baselines would not provide direct evidence to invalidate results from the slope, beta peak time, or ITC analyses, differences in baselines between conditions could account for reported differences in beta peak power between omission and non-omission conditions. Separate paired *t* tests comparing the baseline spectrum in the beta band were computed for each cluster for both induced and evoked activity. All *t* tests used FDR correction to account for multiple comparisons (Benjamini & Hochberg, 1995). Baseline power for the comparisons was taken directly from the time–frequency calculations used in the previous analyses and averaged across the beta band (14–30 Hz) to match the other beta band analyses we report.

4 | RESULTS

4.1 | Channel-level beta slope analysis

Figure 4 depicts the results of these tests at the electrode level show that only channel P8 meets the criteria for the four tests for visual beta: $p > 0.05$ for the omission to non-omission slopes comparison, $p < 0.05$ for the comparisons of the non-omission to shuffled and omission to shuffled slopes, and $p < 0.05$ for the post hoc comparison test as applied to the slopes fitted to the between the trough of beta power and onset for induced beta. Additional channels met the first three criteria but did not reach significance in the post hoc test for the induced trough-fitted slope for both visual and auditory conditions. No channels met these criteria for the slopes fitted at the fixed values between −300 ms and onset for the visual condition for induced or evoked beta. No auditory channels met the four criteria for any of the conditions.

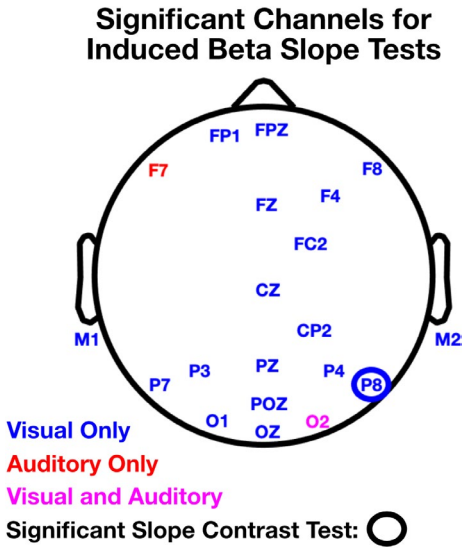

FIGURE 4 Significant channels for the induced beta tests to slopes fitted from the trough of beta power between −300 and −100 ms to the event onset at 0 ms. Channels labeled had $p > 0.05$ for the omission to control slopes comparison, and $p < 0.05$ for the comparisons of the control to shuffled and omission to shuffled slopes. The circled channel indicates $p < 0.05$ for the post hoc comparison test as applied to the slopes fitted to the between the trough of beta power and onset for induced beta

4.2 | Cluster-level analyses

To better separate sensory and timing related activity and to investigate the sources of timing-related activity, we performed the remaining analyses at the cluster level. Due to the large number of tests results from our analyses at the cluster level, we focus on four clusters of interest: the parietal and occipital clusters for the visual condition, and the left and right sensorimotor clusters for the auditory condition. In the visual condition, we focus on the parietal cluster as it shows the strongest visual predictive beta results while producing a beta time course very similar to two of the other posterior clusters: the left and right temporal/parietal clusters. We focus on the occipital cluster for the visual condition as its activity is mostly likely to arise from the visual cortex, yet its markers of predictive activity are not as pronounced as with the other posterior clusters. The left and right sensorimotor clusters are of interest as they are the only clusters that show predictive beta activity exclusively in the auditory modality, and additionally suggest hemispheric differences in auditory rhythm processing. In addition to these clusters, we also present results from the parent cluster for both sensory modalities to provide a global-level view of the beta activity. The test results from all clusters for both modalities, along with figures, are available in Supporting Information.

4.3 | Event-related spectral perturbations

In the parent cluster containing all components, we find increased evoked power following both visual and auditory stimulus onset, but not in response to visual or auditory omission onsets (Figure 5). Induced activity from the visual condition in the parent cluster not only increases significantly and peaks roughly at stimulus onset but also increases at omission onset, particularly in the low beta range. This pattern is also seen in the posterior clusters for visual activity, especially in the parietal cluster (Figure 6a). In the occipital cluster, visual induced beta peaks much closer to the stimulus onset and prior to the omission onset (Figure 6b). Visual-evoked activity for the parietal and occipital clusters follows the same pattern seen in the parent cluster. ERSP power modulation is less pronounced in response to auditory rhythms compared with visual rhythms in the parent cluster with both induced (Figure 5c) and evoked (Figure 5d) measures. Modulation of induced activity appears stronger in response to auditory rhythms in the right sensorimotor cluster (Figure 6d) than the left sensorimotor cluster (Figure 6c). Evoked beta modulation in response to auditory rhythms is relatively weak but appears less affected by an auditory omitted event than seen with the visual clusters, especially in the left sensorimotor cluster (Figure 6c).

4.4 | Beta slope analysis

Slopes were fitted to the cluster-level beta activity with the four previously described tests applied. Figure 7 shows the time course of visual beta activity in the parietal (a) and occipital (b) clusters and auditory beta activity for the left (c) and right (d) sensorimotor clusters for both induced and evoked activity. At the cluster level in the visual modality two clusters plus the parent cluster met the criteria in induced activity for the slopes fitted to −300 to 0 ms: right temporal/parietal and parietal clusters. The left temporal/parietal cluster met the criteria for three of the slope tests but not for the contrast. No auditory clusters met the criteria for induced activity with a fixed slope. Slopes fitted to the trough (between −300 and −100 ms) and 0 ms for induced beta activity in the visual condition resulted in five clusters plus the parent cluster meeting the criteria for the four slope tests: midline central area, right frontal, left temporal/parietal, parietal region, and right temporal/parietal clusters. The occipital cluster met the first three slope criteria in the visual modality for the trough-fitted slope in induced activity. The parietal and the parent cluster met all four criteria for the auditory condition for trough-fitted slopes to induced beta. All other clusters except the midline central area cluster met the first three slope criteria for auditory-induced beta trough-fitted slopes.

Slopes fitted to evoked beta at the cluster level resulted in the parent cluster for both auditory and visual modalities,

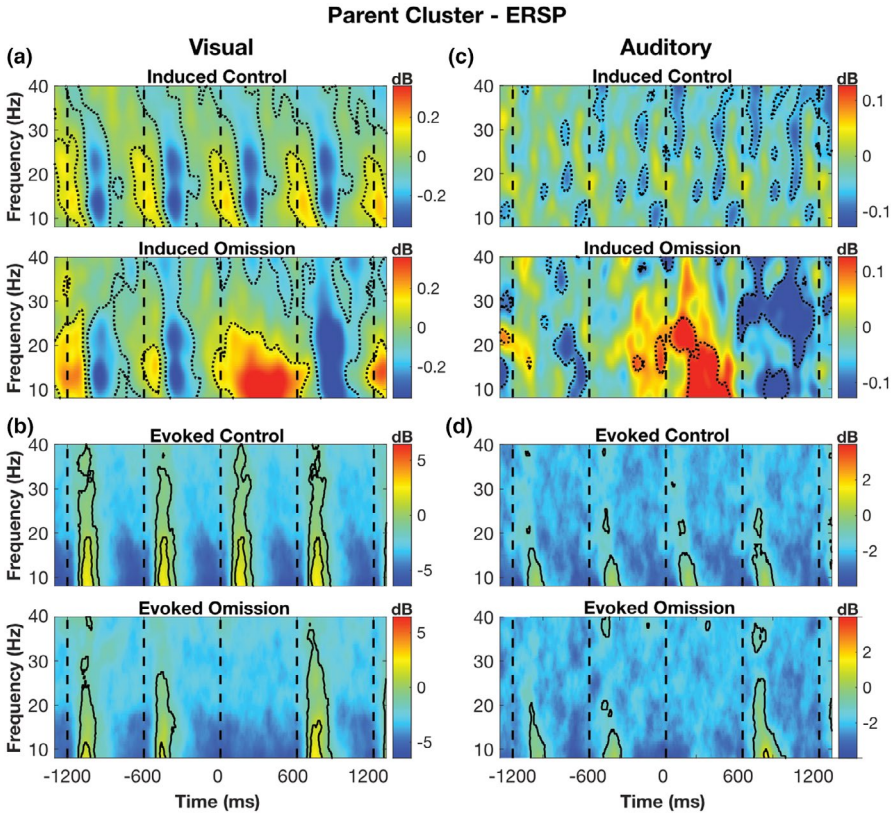

FIGURE 5 Time–frequency dynamics in the parent cluster for visual (a,b) and auditory (c,d) conditions. Data shown are grand averages across all components in the parent cluster, which is made up of all components prior to clustering to present global-level activity. Dotted lines in induced activity (a,c) indicate time–frequency values significantly different from baseline $p < 0.01$. Solid lines in evoked activity (b,d) indicate time–frequency values significantly different from baseline $p < 0.001$. ERSP, event-related spectral perturbation

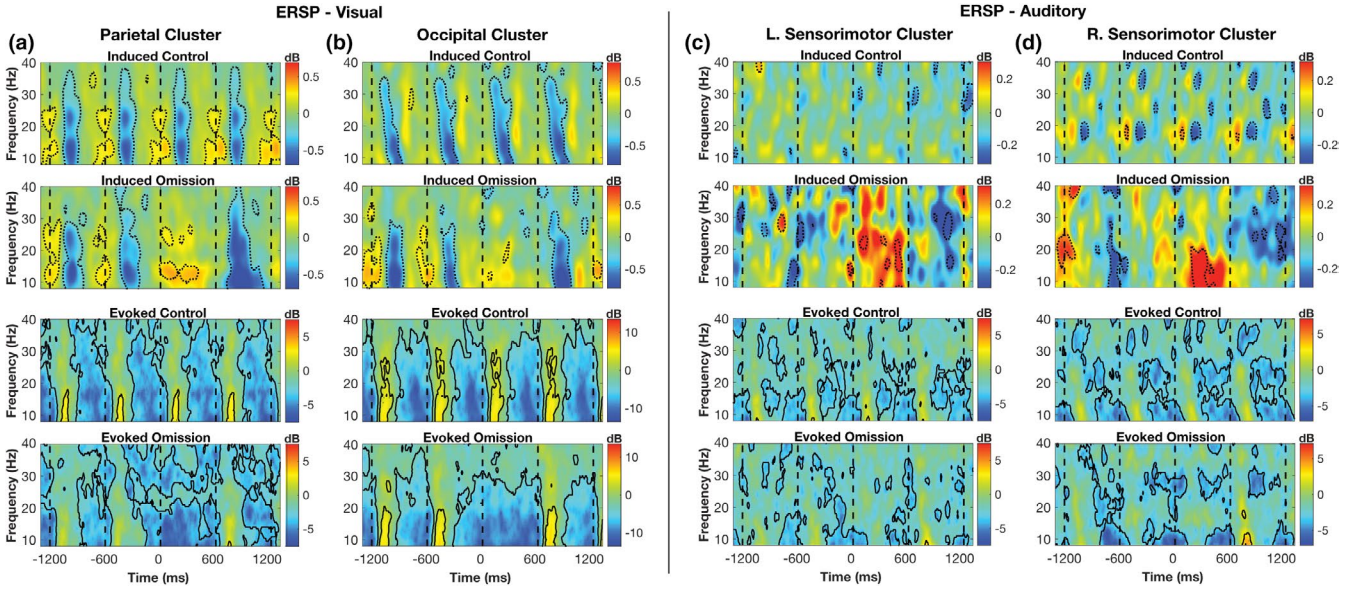

FIGURE 6 Time–frequency dynamics in selected clusters for visual (a,b) and auditory (c,d) conditions. Data shown are grand averages across all components in the indicated cluster. Dotted lines in induced activity indicate time–frequency values significantly different from baseline $p < 0.01$. Solid lines in evoked activity indicate time–frequency values significantly different from baseline $p < 0.001$. Induced and evoked ERSP values in response to visual rhythms from the parietal (a) and occipital (b) clusters, and ERSP values in response to auditory rhythms from the left sensorimotor (c) and right sensorimotor (d) clusters are depicted. ERSP, event-related spectral perturbation

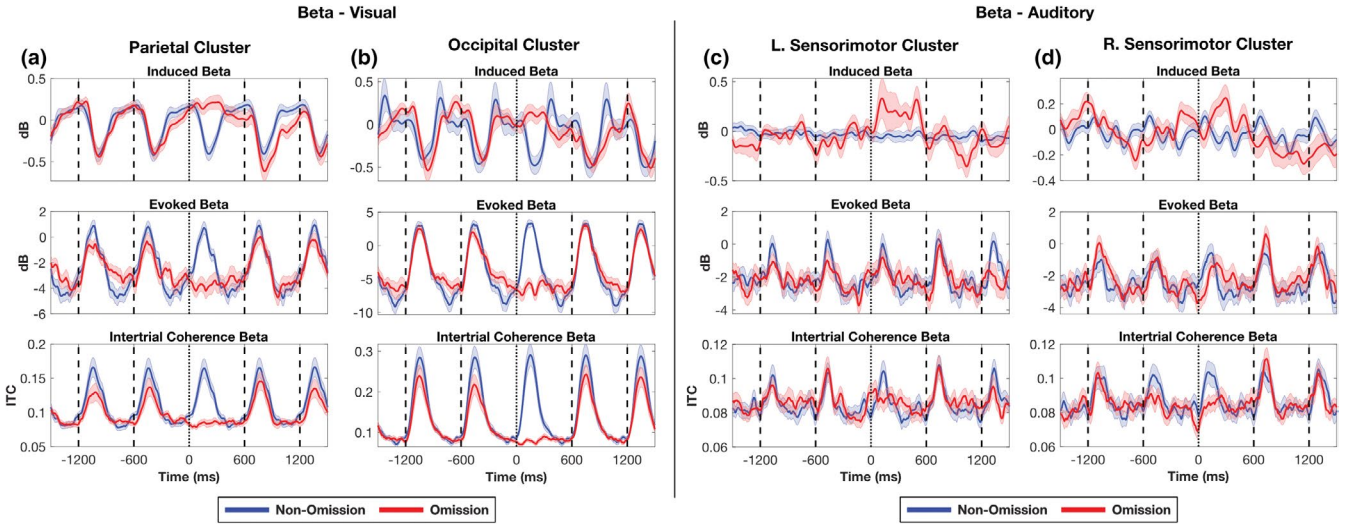

FIGURE 7 Time course of induced and evoked beta activity, and intertrial coherence (ITC) in the beta band for selected clusters in response to visual (a,b) and auditory (c,d) rhythms. Standard error is indicated with shaded bars. Values in response to visual rhythms from the parietal (a) and occipital (b) clusters, and values in response to auditory rhythms from the left sensorimotor (c) and right sensorimotor (d) clusters are depicted. Note that evoked beta and ITC increase in anticipation of an event only in the left sensorimotor cluster (c)

and the left sensorimotor cluster for the auditory modality meeting all four slope criteria for the trough-fitted slopes. The midline central area cluster, right sensorimotor, and parietal cluster met the first three criteria for the trough-fitted slope tests in both modalities. the left temporal/parietal and left frontal cluster in the auditory and visual modalities, respectively, met the first three slope criteria for the trough-fitted slopes. No cluster met any of the necessary criteria in the slopes fitted between −300 and 0 ms to evoked beta activity. All slope measures and tests for the visual and auditory slopes can be found in the Tables S1 (visual) and S2 (auditory).

4.5 | Induced and evoked beta peaks

Test values presented here are for the parent cluster containing all components unless otherwise indicated. For a full listing of all test values and statistics for each cluster, refer to Tables S3 (visual peak times), S4 (visual peak power), S5 (auditory peak times), and S6 (auditory peak power). Figure 8 shows the distribution of visual beta peak times and power for the parietal and occipital clusters. Figure 9 shows the distribution of auditory beta peak times and power for the left and right sensorimotor clusters. In the visual modality, evoked peak times for the control condition were generally after flash onset (M = 68.49 ms, SD = 122.18) and later than omission peak times (M = 11.04 ms, SD = 133.51); $t(288)$ = 5.43, p = <0.001. Visual-induced peak times for the control condition tended to fall prior to onset (M = −12.95 ms, SD = 120.03), whereas omission peak times fell after expected onset (M = 28.74 ms, SD = 129.27); $t(288)$ = −4.47, p = <0.001. Both tests were also significant for the midline central area and parietal cluster, with the left temporal/parietal cluster significant in induced activity and the right temporal/parietal cluster significant for evoked. The evoked control peak was significantly later than the induced control peak; $t(288)$ = 8.06, p = <0.001. This difference was also reflected in the midline central area, right frontal, left temporal/parietal, occipital, parietal, and right temporal/parietal clusters. Evoked and induced omission peak times were not significantly different in the parent cluster ($t(288)$ = −1.67, p = 0.164) or any other cluster. To determine if the differences in control and omission peak times across induced and evoked activity were relative for each kind of activity, a further test compared the difference in evoked control and omission peak times (M = 57.44 ms, SD = 178) to the difference in induced control and omission peak times (M = −41.68 ms, SD = 158.43), revealing the relative shifts were significantly different; $t(288)$ = 7.03, p = <0.001. A significant relative difference was also seen in the midline central area, left temporal/parietal, occipital, and parietal clusters.

The same tests were run on the auditory beta peak times, revealing that evoked auditory peak times for control (M = 10.64 ms, SD = 122.49) and omission (M = −2.23 ms, SD = 131.29) and induced auditory peak times for control (M = 0.35 ms, SD = 129.6) and omission (M = 6.7 ms, SD = 135.51) conditions were generally close to onset time

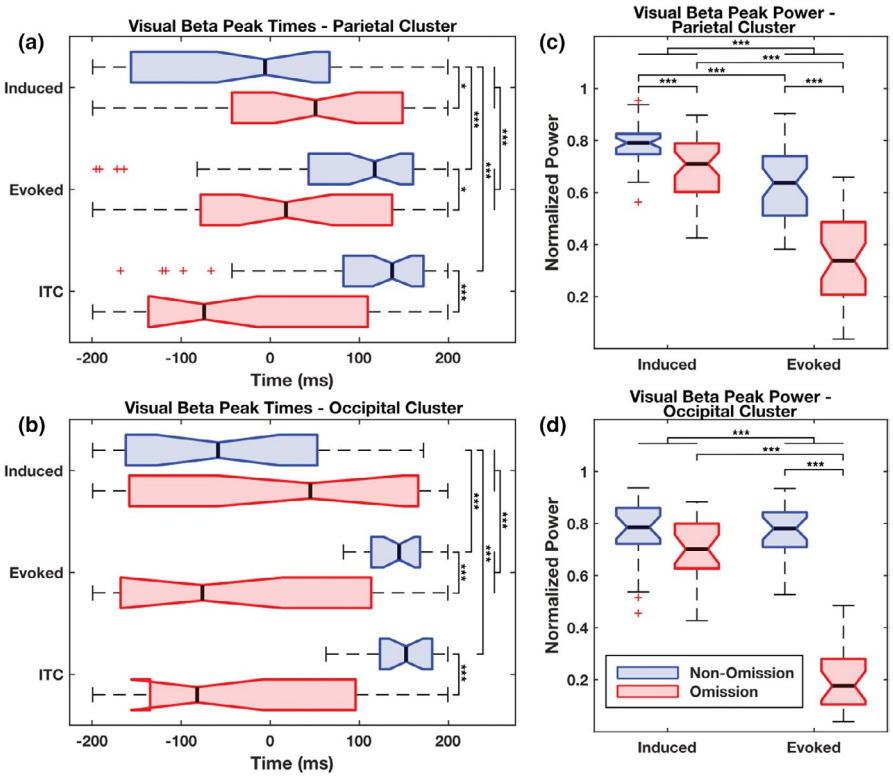

FIGURE 8 Mean beta peak times (a,b) and normalized beta peak power (c,d) for components in the parietal (a,c) and occipital clusters (b,d) in the visual condition. Induced activity for both clusters tended to peak prior to non-omitted flash onset and after omitted flash onsets, whereas the opposite pattern is seen in evoked activity and in intertrial coherence (ITC) (a,b). Normalized induced and evoked beta power peaks were higher in non-omission trials compared with omission trials in the parietal cluster (c), whereas only evoked beta power peaks were higher in non-omission trials than omission trials in the occipital cluster (d). Box plots depict interquartile range with median values indicated by black bars and 95% confidence intervals indicated with notches. Significance differences are shown through bars where *p < 0.05, ***p < 0.001

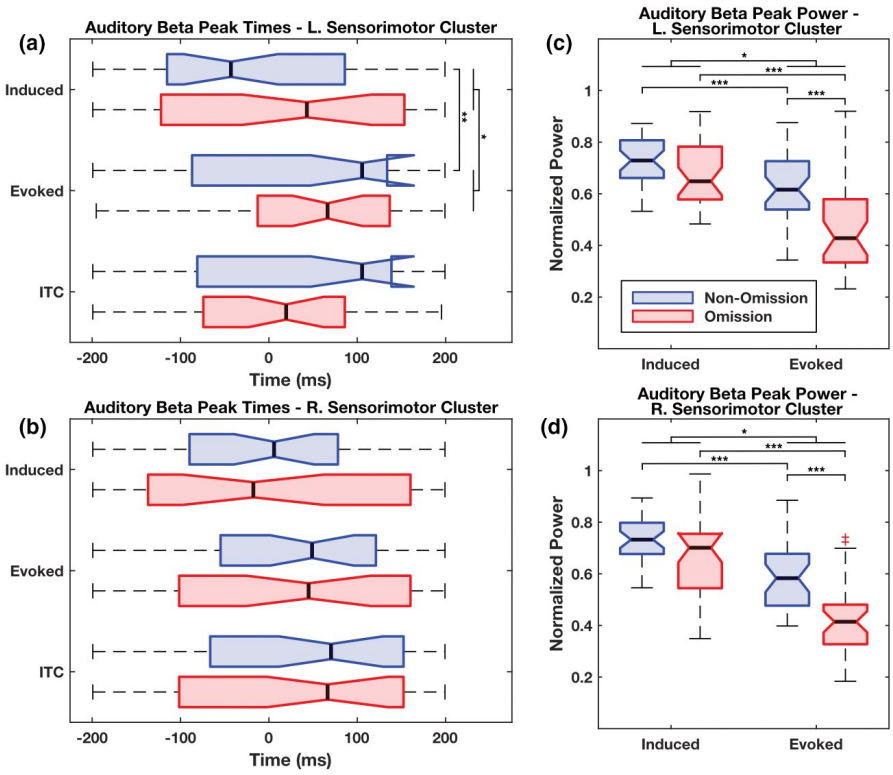

FIGURE 9 Mean beta peak times (a,b) and mean normalized beta peak power (c,d) for components in the left sensorimotor (a,c) and right sensorimotor clusters (b,d) in the auditory condition. In the left sensorimotor cluster (a) induced beta peaked prior to tone onset in the non-omission trials, but after expected onset in omission trials. Note that evoked and intertrial coherence (ITC) beta peak times appear less variable in response to omitted tone than to non-omitted tones in the left sensorimotor cluster (a), whereas beta peak times were especially variabile in the right sensorimotor cluster (b). Normalized beta peak power shows the same pattern in both left (c) and right (d) sensorimotor clusters with power lower in the evoked omission trials compared with the evoked non-omission trials and overall lower evoked power than induced power. Box plots depict interquartile range with median values indicated by black bars and 95% confidence intervals indicated with notches. Significance differences are shown through bars where $*p < 0.05$, $**p < 0.01$, $***p < 0.001$

and not significantly different from each other across all clusters and all tests except for the left sensorimotor cluster, where evoked control peak time ($M = 64.96$, $SD = 124.59$) was significantly later than induced control peak time ($M = -23.44$, $SD = 122.23$); $t(34) = 3.27$, $p = 0.006$ (Figure 9a). The difference between evoked control and omission peak times ($M = 35.38$, $SD = 167.02$) and the difference between induced control and omission peak times ($M = -45.42$, $SD = 151.1$) was also found to be significant in the left sensorimotor cluster; $t(34) = 2.39$, $p = 0.047$ (Figure 9a).

Visual modality-evoked control peak values ($M = 0.631$, $SD = 0.141$) were greater than evoked omission peak values ($M = 0.366$, $SD = 0.163$); $t(288) = 20.04$, $p = <0.001$. Similarly, visual modality-induced control peak values ($M = 0.753$, $SD = 0.117$) were greater than induced omission peak values ($M = 0.664$, $SD = 0.136$), although to a lesser degree; $t(288) = 9.58$, $p = <0.001$. The comparison tests across visual omission and non-omission peak values within evoked and induced activity were significant for all clusters. Comparisons across evoked and induced peak values for visual beta indicated induced non-omission peaks were generally larger than evoked non-omission peaks; $t(288) = -13$, $p = <0.001$. This comparison was found to be significant for all clusters except the occipital cluster (Figure 8d). Comparisons across visual beta evoked and induced omission-fitted peak values indicate induced omission peak values are greater than evoked omission peak values for the parent cluster; $t(288) = -23.99$, $p = <0.001$, and all other clusters. A comparison between the difference in evoked non-omission and omission peak power ($M = 0.264$, $SD = 0.224$) and the difference between induced non-omission and omission peak power ($M = 0.089$, $SD = 0.157$) indicated a greater relative difference was seen in evoked activity for the parent cluster ($t(288) = 11.24$, $p = <0.001$), as well as for clusters 3 (mid central), 5 (right frontal), 8 (parietal), and 9 (right temporal/parietal).

Running the same tests on auditory peak values show auditory evoked non-omission peak power ($M = 0.592$, $SD = 0.125$) was significantly greater than auditory evoked omission peak power ($M = 0.442$, $SD = 0.146$) for the parent cluster ($t(288) = 13.24$, $p = <0.001$), and all other clusters except for the midline central area cluster. Auditory-induced non-omission peak power ($M = 0.73$, $SD = 0.099$) was slightly larger than auditory-induced omission peak power

($M = 0.677$, $SD = 0.124$), and significantly so for the parent cluster ($t(288) = 5.72$, $p = <0.001$), as well as for the midline central area, occipital, and right temporal/parietal clusters. A comparison across auditory-evoked and auditory-induced non-omission peak power reveals induced non-omission peak power is significantly greater in the parent cluster ($t(288) = -15.65$, $p = <0.001$), as well as in all other clusters except the left frontal cluster. Auditory-induced omission peak power was found significantly larger in the parent cluster ($t(288) = -20.27$, $p = <0.001$), as well as all other clusters. Comparing the difference in evoked non-omission and omission peak power ($M = 0.15$, $SD = 0.193$) and the difference between induced non-omission and omission peak power ($M = 0.053$, $SD = 0.156$) revealed a greater relative difference in evoked activity that was significant in parent cluster ($t(288) = 6.51$, $p = <0.001$), as well as for the left sensorimotor, right sensorimotor, right frontal, and parietal clusters.

4.6 | Intertrial coherence

The time course of ITC in the beta band for the parietal and occipital clusters in the visual condition, and in the left and right sensorimotor clusters in the auditory condition is depicted in the bottom row of plots in Figure 7, where ITC can be compared against evoked and induced beta activity. The distribution of ITC peak times for the aforementioned clusters are depicted in Figures 8a,b (visual) and 9a,b allowing for a comparison against evoked and induced peak times. No significant differences were found between ITC beta peak times and evoked beta peak times for either auditory or visual conditions in any cluster. Comparisons between ITC beta peak times and induced beta peak times showed induced beta peaked prior to the peak in ITC beta in the non-omission condition in the visual modality in the parent cluster ($t(288) = 8.5$, $p = <0.001$), left temporal–parietal cluster ($t(27) = 3.7$, $p = 0.012$), right temporal–parietal cluster ($t(28) = 5.28$, $p = <0.001$), parietal cluster ($t(41) = 5.59$, $p = <0.001$), occipital cluster ($t(23) = 9.83$, $p = <0.001$), and right frontal cluster ($t(38) = 3.46$, $p = 0.015$). Additionally, ITC beta peaked earlier than induced beta in the visual omission condition in the parent cluster ($t(288) = -2.83$, $p = 0.042$). There were no significant differences between induced beta peak times and ITC beata peak times in the auditory conditions. Non-omission ITC beta peaked later than omission ITC beta in the visual modality in the parent cluster ($t(288) = 7.7$, $p = <0.001$), left temporal–parietal cluster ($t(27) = 3.17$, $p = 0.035$), right temporal–parietal cluster ($t(28) = 4.79$, $p = <0.001$), parietal cluster ($t(41) = 4.81$ $p = <0.001$), occipital cluster ($t(23) = 5.72$, $p = <0.001$). In the auditory condition, non-omission ITC beta peaked later than omission ITC beta in the parent cluster ($t(288) = 3.16$, $p = 0.017$).

4.7 | Baseline activity

The comparison of baseline power revealed no significant differences in the majority of the tests. The comparisons that do show differences are predominantly relegated to the parent cluster, and the left and right frontal clusters for both modalities. Additional differences were seen in the visual modality in induced beta in the parietal cluster and evoked beta for the occipital cluster. All instances of significant differences between baselines show reduced power in the non-omission baseline compared with the omission baseline with the exception of the occipital cluster. All test values and statistical results of the baseline analysis are listed in Tables S7 and S8.

5 | DISCUSSION

5.1 | Summary of results

Using an IC cluster-based approach for isolating network-level beta band activity, we describe predictive timing in a modality-specific way. Analyses on the slopes of beta activity from the parent clusters reveal evidence for both induced and evoked predictive timing in auditory and visual modalities at the global level. The slopes of beta activity from individual clusters indicates evidence of induced predictive timing in the visual modality in posterior regions: left and right temporal/parietal clusters, and parietal cluster; the midline central cluster, and from the right frontal cluster. Slope-based evidence for induced predictive timing in the auditory modality was found in the parietal cluster. Cluster-specific evidence of evoked predictive timing in slope measures was seen only in the auditory modality, in the left sensorimotor cluster.

It would be expected, based on Snyder and Large (2005), that evoked beta peak power would be significantly lower for omission events compared with tone or flash events and that there would be no significant difference in induced beta peak power between omission events and tone or flash events. This pattern was seen much more prominently in the auditory modality, specifically in the parietal, left and right sensorimotor, left and right frontal, and left temporal/parietal clusters. A significant difference would additionally be expected between how much evoked beta peak power shifted between non-omission and omission conditions and how much induced beta power shifted between non-omissions and omissions. This significant difference was replicated in several clusters: the parietal cluster, left and right sensorimotor clusters, and the right frontal cluster, thus providing strong evidence for auditory-induced beta playing a predictive role in networks of those regions. There were a few differences in the peak times in auditory beta across both induced and evoked activity and conditions. The significant shift in peak time from tone to omitted tone trials between induced and

evoked beta for the right sensorimotor cluster follows the expected pattern of induced beta peaking later in response to an omitted tone than in response to a non-omitted tone. The evoked beta peaked earlier in response to an omitted tone than in response to a non-omitted tone. Although not significant, we find it interesting that the opposite pattern with beta peak time appears in the left sensorimotor cluster: induced beta peaked slightly earlier in response to omitted tones than in response to tones, yet evoked beta peaked slightly later in response to the omitted tones than in response to the tones. This is in concordance with what would be expected if evoked beta was playing a predictive role, and when taken in conjunction with the slope evidence of predictive evoked activity in the left sensorimotor cluster suggests the existence of significant hemispheric differences in auditory rhythm processing mechanisms. The findings indicating no significant difference between auditory evoked beta peak times and ITC beta peak times suggests the hemispheric differences seen in the sensorimotor clusters are a result of phase resetting in the beta band anticipating the onset of the auditory event. The baseline analyses showing no significant differences for the sensorimotor and parietal clusters indicate the beta peak power differences are not due to any habituation effect. Although we do see a baseline difference in the right frontal cluster, the baseline differences only directly affect the non-omission to omission comparisons, and not the within condition comparisons, for example, non-omission-induced beta peak power compared with non-omission-evoked beta peak power. Furthermore, when taking into account that the beta peak power results of the right frontal cluster closely match those reported by Snyder and Large (2005), they are likely to represent a genuine effect, indicating auditory beta timing in a left frontal region.

Differences in evoked and induced beta power in response to visual non-omissions and omissions did not provide clear evidence of predictive beta as seen in the auditory case, except for in the shift of peak power between evoked and induced activity from flash-to-flash omission in the parent, parietal, midline central, right frontal, and right temporal/parietal clusters. Interestingly, a look at differences in peak times does provide stronger evidence suggesting separate roles for evoked and induced beta for the parietal, right and left temporal/parietal, and occipital clusters. In these clusters, the evoked beta peak came earlier in response to omitted flashes than to non-omitted flashes, whereas induced beta peaked later in response to omitted flashes than to non-omitted flashes, which is what would be expected if induced beta activity was playing a predictive role, whereas evoked beta was only responsive to stimuli. The significant differences between ITC beta peak times and induced beta peak times in the left and right temporal-parietal clusters, parietal cluster, and occipital cluster combined with the no significant differences between ITC and evoked beta peak times add further evidence for the role of predictive beta activity. Although we do see baseline differences in the visual modality for the parietal, occipital, and right frontal clusters, those differences do not provide evidence to invalidate our findings because the slope-based and beta peak time evidence from those clusters would not be directly affected by baseline differences. Taken together with the slope results, we interpret these findings as evidence of induced beta playing a predictive role in visual rhythm perception similar to that reported in previous studies for auditory-induced beta (Fujioka et al., 2009, 2012, 2015; Snyder & Large, 2005). The overall pattern indicates induced beta power rising in anticipation of an incoming tone or flash. In response to the flash onset, we see phase resetting in the beta band as indicated by increased ITC, resulting in increased evoked activity. This increase in evoked activity appears to act as a marker to reset the anticipatory timing seen in induced beta such that induced beta power drops before beginning its rise in anticipation of the next event. When an event is omitted, there is little to no phase resetting seen and so induced beta continues to rise and plateau before eventually falling until the next event causes the induced beta power to drop further and thus restarting the cycle.

If we take together the findings from the beta slope tests and the beta peak power and time tests, we find evidence of predictive visual beta in the left and right temporal/parietal clusters, the occipital cluster, the midline cluster, the parietal cluster, and the right frontal cluster. These tests show evidence of predictive auditory beta in the left and right sensorimotor clusters, the right frontal cluster, and parietal cluster. The results taken all together suggest the existence of modality independent, but possibly overlapping networks for rhythm timing (Figure 10).

5.2 | Predictive beta band activity

Beta modulation has been shown to play a role in a wide range of activities including top-down control on sensorimotor systems (Arnal et al., 2011; Engel & Fries, 2010; Haegens & Golumbic, 2018; Picazio et al., 2014), facilitating long-range communication between cortical regions (Kilavik et al., 2013; Kopell et al., 2000) such as between sensorimotor and peripheral areas (Fujioka et al., 2015), and is suggested to play a role in encoding temporal intervals (Wiener & Kanai, 2016). Beta band activity also correlates with motor behavior, with power attenuation just before and during movements (see Kilavik et al., 2013 for review). Considering the suggested role, the motor cortex has in timing and predictive processing (Patel & Iversen, 2014; Schubotz et al., 2000), the role of beta in imposing general top-down control, and its role in facilitating communication

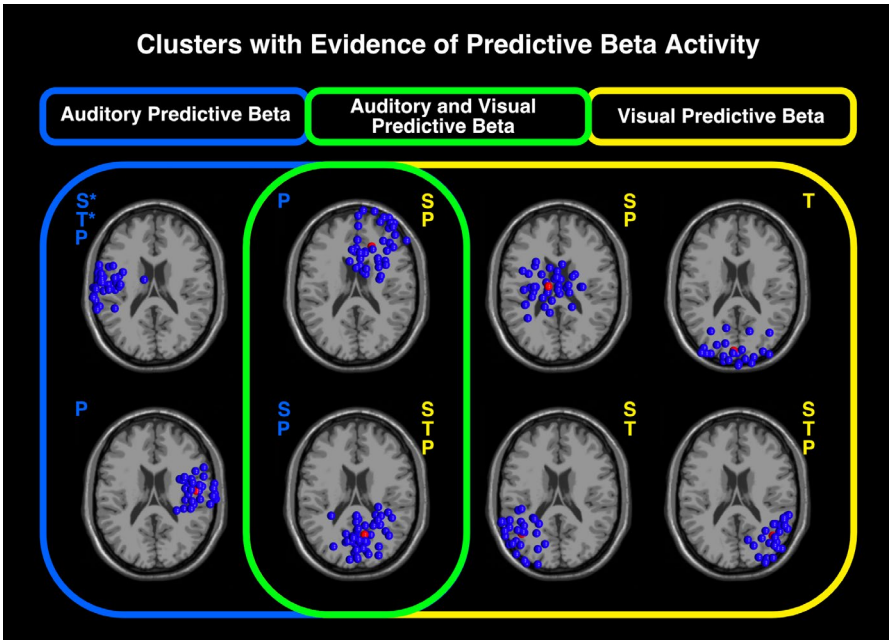

FIGURE 10 Overview of clusters with evidence of predictive beta activity for auditory and visual rhythm processing indicated. Clusters within the blue area show predictive activity for only auditory rhythms, clusters within the yellow for only visual rhythms, and clusters within the green areas for both auditory and visual rhythms. The type of predictive evidence is listed for each cluster with evidence for visual rhythms in yellow and auditory rhythms in blue. All predictive evidence was in induced beta activity except for auditory rhythms in the left sensorimotor cluster where evidence of predictive evoked beta activity was found. P, peak power evidence of predictive beta; S, slope evidence of predictive beta; T, peak time evidence of predictive beta. *Predictive evoked beta

with sensorimotor peripheral systems, it is not surprising that beta activity appears to play a role in rhythm perception and prediction.

Beyond the link to sensorimotor behavior, beta activity is known to play a role in auditory rhythm perception. Frontocentral-induced beta and gamma modulation occurs with the onset of rhythmic events and can be seen at the expected onset of an omitted event (Snyder & Large, 2005). Fujioka et al. (2012) found that beta power arising from the auditory cortices increases before tone onset in an isochronous rhythm at a rate dependent on the tempo of the rhythm and attenuates following the tone at a constant rate not dependent on the tempo of the rhythm. Beta activity has also been seen to play a role in maintaining beat and meter (Fujioka et al., 2015). Consistent with these findings, we find evidence of auditory-induced beta power peaking in anticipation of both tones and omitted tones, with the strongest evidence coming from the parietal, left and right sensorimotor, and right frontal clusters. Because the source of neural activations are more difficult to localize using EEG than MEG, some caution is needed in interpreting the location of these sources. However, given other findings suggesting predictive induced beta arising from frontocentral regions using EEG (Snyder & Large, 2005), and from the auditory cortices, sensorimotor cortices, and parietal cortices using MEG (Fujioka et al., 2012, 2015), we believe the regions indicated by the cluster locations are reasonable interpretations of the source of the predictive beta we measured. It is of note that we did not find evidence of predictive beta that we could tie clearly to the auditory cortex. This may be a limitation of the EEG IC cluster approach we used; it has been put forth that signals arising from the auditory cortex are more suited to being measured by MEG than EEG (Destoky et al., 2019).

When looking at beta modulation in the visual domain, we see a beta power increase at the expected onset of an omitted flash in multiple clusters. Comparing beta modulation in anticipation of the visual onset between the omission and non-omission conditions shows induced beta power increasing prior to onset, followed by a sharp power drop-off, but only after flash onset, and not following omission onset. Although we expected to find predictive beta activity in the visual domain, it was surprising to see evidence of predictive induced beta modulated more clearly and across more clusters in the visual domain than in the auditory domain because the timing aspects of rhythm perception in the auditory domain are thought to be more precise as evinced by less variability in auditory SMS compared to visual SMS (Repp, 2005, Repp & Su, 2013). The discrepancy between auditory and visual beta modulation may be due to auditory signals being more suited to measurement from MEG than from EEG (Destoky et al., 2019), resulting in a comparatively reduced measurement of beta modulated by auditory rhythms. The apparent size difference between the auditory and visual cortex may play an additional role.

The clusters that show evidence of predictive beta activity for the visual modality do not perfectly overlap with what is seen in the auditory modality. In the sensorimotor clusters, we only find evidence of auditory predictive beta in bilateral sensorimotor clusters, and not visual predictive beta. There is evidence of visual predictive beta in the midline cluster, which contains dipoles localized to the premotor regions. This may indicate motor system involvement and would be in line with research suggesting the medial premotor region plays a role in predictive timing in primates across sensory modalities (Merchant et al., 2013). However, this begs the question of why the same activity was not seen in the auditory modality if premotor timing activity is not modality specific. A possible explanation is given by work reporting that a greater number of cells in the primate SMA respond to visual timing cues than to auditory timing cues (Merchant et al., 2015), although it is not clear if this finding extends to humans or if it is specific to the primates involved in that study. It is also of interest that we find predictive visual-induced beta activity from the slope analysis in left and right temporal/parietal junction and parietal clusters, but not in the occipital cluster. Given the difficulty in localizing sources with EEG, and the component distribution of the four posterior clusters, it is likely the left and right temporal/parietal and parietal clusters contain activity arising from cortical patches within the occipital cortex. Considering the distribution of components, and the faster rebound in induced beta power in the occipital cluster (Figure 5b), we consider it likely that activity from early processing areas of the visual cortex (e.g., V1) are more strongly represented in the occipital cluster than the surrounding posterior clusters. This, however, cannot be confirmed with the spatial limitations of EEG and will require a methodology with greater spatial precision to test.

Although beta power modulation in response to visual rhythmic flashes has been seen before (Meijer et al., 2016; Saleh et al., 2010), to our knowledge this is the first time it has been shown predicting the onset of an omitted event. However, it has been questioned whether beta modulation is even related to temporal prediction at all (Meijer et al., 2016). Meijer et al. (2016) investigated beta activity with a rhythmic visual task and found beta power modulation in response to isochronous visual rhythms of different tempi (IOI's of 1,050, 1,350, 1,650 ms), yet the rate of beta power modulation was the same regardless of the tempo used. This is different from what was found by Fujioka et al. (2012) in their study of auditory beta modulation, where the rate of beta power prior to tone onset was modulated by the tempo of the rhythm. Meijer et al. (2016) interpreted their result as evidence that beta activity is not playing an entraining role in the visual system, suggesting instead that the beta peaks seen may be caused by rebounding activity in response to the flash, peaking roughly 900 ms after event onsets. The current study provides the contrary evidence and suggests that beta modulation may be playing a role in prediction of the onset of visual events because the beta modulation during the omission could not be in response to any event and instead must be responding to the timing of the expected onset of the flash. Induced beta peaks <50 ms after the omission onset, or 650 ms after the onset of the prior stimulus (Figure 4), which is much earlier than would be expected for beta power rebound in response to the flash event, as described by Meijer et al. (2016). We suggest the reason for the discrepancy between Meijer et al.'s (2016) findings and those findings reported here may be due to their use of relatively slow tempi compared with the 600 ms IOI of this study. Additionally, the task used in the Meijer et al. (2016) study was much more complicated than simply attending to the timing of the rhythms as in our task and demanded more attention and possibly competing resources. There is evidence that sub-second timing and supra-second timing use different networks (see Wiener et al., 2010 for a review). We, therefore, suggest beta synchronization may only be playing a predictive role in the sub-second time scale.

5.3 | Contribution of the motor system

Previous studies have described induced beta modulation to auditory rhythms arising from sensorimotor cortices (Fujioka et al., 2012, 2015). There is also evidence that auditory timing appears to rely on motor cortex (Iversen & Balasubramaniam, 2016; Janata et al., 2012; Repp & Su, 2013; Ross, Iversen, et al., 2016; Ross, Warlaumont, et al., 2016) and motor networks with nodes in the parietal lobes, cerebellum, and basal ganglia (Levitin et al., 2018; Patel & Iversen, 2014; Repp & Su, 2013). This motor network activity could indicate that the motor system is playing an important role in predicting the timing of events in auditory rhythms, often discussed in the context of evolution of social activities such as dance and language (Fitch, 2016; Iversen, 2016; Patel, 2006). The auditory beta modulation from the sensorimotor clusters we present here is consistent with the narratives of the previous literature on the involvement of the motor system for auditory timing. This can be contrasted with our findings from the visual system where there is no evidence of predictive beta timing in the bilateral sensorimotor clusters and instead evidence in the mid-central cluster that may be related to activity arising from the SMA.

In the auditory modality, we found evoked predictive beta timing activity in the left sensorimotor cluster (Figure 6a), yet we found evidence of induced predictive timing activity in the right sensorimotor cluster (Figure 7a). The asymmetrical beta activity seen in the two sensorimotor clusters specific to the auditory conditions suggests hemispheric specialization specific to auditory processing. A recent meta-analysis on neural activation during music listening shows consistent

MRI activation in the right but not left primary motor cortex during music listening tasks (Gordon et al., 2018). Interestingly, they found that studies that asked the subjects to move a body part while listening elicited stronger activity in the right primary motor cortex than studies using passive listening tasks. Others describe a left hemisphere role (Pollok et al., 2008) or non-motor-dominant hemisphere role (Kaulmann et al., 2017; Yadav & Sainburg, 2014) for motor timing. Similarly, for language perception there appears to be hemispheric specialization in the auditory cortices, with the left hemisphere specialized in temporal changes and the right hemisphere in spectral changes (Zatorre & Belin, 2001; Zatorre et al., 1992). Specifically, it has been shown that activity in the left anterolateral superior temporal sulcus (STS) corresponds to processing of temporal aspects of speech perception, whereas perception of spectral features of speech are associated with the same structure in the right hemisphere (Obleser et al., 2008). Our results support bilateral motor contributions to auditory timing, although the mechanism that results in predictive evoked activity in the left hemisphere and induced beta activity in the right hemisphere may be distinct. In particular, the predictive evoked activity seen in the left sensorimotor cluster suggests a timing mechanism driving phase resetting at the expected tone onset not seen in the right sensorimotor cluster or any other cluster.

5.4 | Limitations and future directions

The current study reveals that timing and prediction for visual rhythm perception could use non-motor networks. We cannot say what role, if any, the motor system plays in visual timing. A closer look at the connections between visual and motor systems is needed to elucidate the issue. Using moving visual rhythms as opposed to flashing visual rhythms may elicit a different picture of activation as the visual system is better tuned to discerning temporal information when movement is present (Hove, Iversen, et al., 2013).

Another limitation of the current study is that we did not use multiple tempi. Having only one tempo makes it unclear how much the change in time course of neural activations is related to the tempo. Using multiple rhythms with different tempi would allow for a clearer differentiation between tempo-dependent aspects of timing. If those tempi spanned both sub-second and supra-second interstimulus intervals, this would also provide insight to the temporal limits to the mechanisms in visual rhythm perception.

Although we see frequency band-specific oscillatory modulation during rhythm perception, caution should be used in assuming this is the brain's mechanism of timing. There is evidence for multiple mechanisms for timing (for review see Comstock et al., 2018; Wiener & Kanai, 2016; Wiener et al., 2010), and here we describe one reflection of these processes. Oscillatory dynamics likely reflect more broadly the mechanism for spreading information between or across networks, and timing perception is only a subset of neural communication happening during these tasks.

Additional investigation is needed into the differences seen between left and right motor contributions to auditory timing. Although the differences suggest possible functional lateralization in auditory rhythm perception, it is unclear if those differences are driven by handedness (Kaulmann et al., 2017; Yadav & Sainburg, 2014) or other factors (Pollok et al., 2008). Future studies are needed to look more closely at specific hemispheric contributions.

The inherent low spatial resolution of EEG limits how confidently we can draw conclusions about neural sources. We describe broad cortical source regions/networks in lieu of more focal sources with respect to this methodological limitation but argue that the ICA-based cluster analysis leads to reasonable spatial and functional grouping of neural activity likely from common sources. That being said, we cannot speak with certainty about the exact cortical sources of the activity we describe. A method with better spatial resolution that retains fine temporal resolution, such as MEG or ECoG, would provide better source resolution for predictive rhythm perception networks.

The baseline differences we find in some clusters suggest habituation to the non-omission condition not seen in the omission condition. Although these baseline differences do not directly impact many of the analyses used, nor impact our main findings, they do suggest that future studies should be designed in such a way to avoid unequal habituation to the signal. We also cannot rule out the possibility that unequal baselines could reflect differences in neural activation that may have indirect effects on neural dynamics. We think it unlikely that such differences would impact neural activity in such a way to impact our findings; however, study designs that avoid this possible confound would produce stronger results.

Finally, the nature of this work was primarily to investigate and explore predictive timing markers across auditory and visual modalities in beta activity. Although the exploratory work is often a necessary step in surveying the landscape of a given problem, it can be prone to interpretive biases. For this reason, the exploratory portions of our work should be taken primarily as a guide for further experiments to understand predictive beta activity and differences between the mechanisms of auditory and visual rhythm perception.

6 | CONCLUSIONS

We investigated the mechanisms of prediction for auditory and visual rhythms using an omission paradigm. In confirmation of our hypotheses, the results described here

support theories of predictive timing in both visual and auditory modalities, that can be observed in beta band oscillatory activity. Using an exploratory ICA spatial cluster-based approach, our results also support that visual and auditory prediction for rhythmic events may be subserved by modality-specific cortical networks, although we cannot rule out the possibility that both auditory and visual networks are subserved by a common subcortical network. We describe all clusters resulting from the blind source separation technique in detail, and these results suggest induced beta activity predicting the expected onset of visual rhythmic events bilaterally in temporal/parietal clusters, in a dorsal medial cluster, a parietal cluster, and a right hemisphere frontal cluster. We also show evidence for induced beta activity predicting the expected onset of rhythmic auditory events bilaterally in sensorimotor clusters, in a parietal cluster, and in a right hemisphere frontal cluster, and evidence for evoked auditory predictive timing in a left motor cluster. These findings suggest that auditory timing may involve hemisphere-specific activity, and reliance on motor networks not seen in visual timing.

ACKNOWLEDGMENT

The work was supported by NSF grant BCS 1626505.

CONFLICT OF INTEREST

The authors do not have any conflicts of interest to declare.

AUTHOR CONTRIBUTIONS

DCC and RB conceived and designed this study together. DCC ran all participants and conducted the original analyses. DCC and JMR conducted follow-up analysis. DCC, JMR, and RB co-wrote the paper.

PEER REVIEW

The peer review history for this article is available at https://publons.com/publon/10.1111/ejn.15314.

DATA AVAILABILITY STATEMENT

EEG data, code, and stimuli from this study are available at https://openneuro.org/datasets/ds002218. The EEGLAB (v14.1.1) tools that were used to analyze all the data can be downloaded from the Swartz Center for Computational Neuroscience website: https://sccn.ucsd.edu/eeglab/download.php. Paradigm software (ver. 2.5.0.68) was used to present the instructions and stimuli and to sync the start of each trial with the EEG data.

ORCID

Daniel C. Comstock https://orcid.org/0000-0001-5861-0838

REFERENCES

Abbott, N. T., & Shahin, A. J. (2018). Cross-modal phonetic encoding facilitates the McGurk illusion and phonemic restoration. *Journal of Neurophysiology*, *120*(6), 2988–3000. https://doi.org/10.1152/jn.00262.2018

Araneda, R., Renier, L., Ebner-Karestinos, D., Dricot, L., & De Volder, A. G. (2017). Hearing, feeling or seeing a beat recruits a supramodal network in the auditory dorsal stream. *European Journal of Neuroscience*, *45*, 1439–1450. https://doi.org/10.1111/ejn.13349

Arnal, L. H., Wyart, V., & Giraud, A. L. (2011). Transitions in neural oscillations reflect prediction errors generated in audiovisual speech. *Nature Neuroscience*, *14*(6), 797. https://doi.org/10.1038/nn.2810

Bastos, A. M., Vezoli, J., Bosman, C. A., Schoffelen, J.-M., Oostenveld, R., Dowdall, J. R., De Weerd, P., Kennedy, H., & Fries, P. (2015). Visual areas exert feedforward and feedback influences through distinct frequency channels. *Neuron*, *85*(2), 390–401. https://doi.org/10.1016/j.neuron.2014.12.018

Benjamini, Y., & Hochberg, Y. (1995). Controlling the false discovery rate: A practical and powerful approach to multiple testing. *Journal of the Royal Statistical Society: Series B (Methodological)*, *57*(1), 289–300.

Chang, C. Y., Hsu, S. H., Pion-Tonachini, L., & Jung, T. P. (2018, July). *Evaluation of artifact subspace reconstruction for automatic EEG artifact removal*. In 2018 40th Annual International Conference of the IEEE Engineering in Medicine and Biology Society (EMBC), IEEE (pp. 1242–1245).

Chen, Y., Repp, B. H., & Patel, A. D. (2002). Spectral decomposition of variability in synchronization and continuation tapping: Comparisons between auditory and visual pacing and feedback conditions. *Human Movement Science*, *21*, 515–532. https://doi.org/10.1016/S0167-9457(02)00138-0

Comstock, D. C., & Balasubramaniam, R. (2018). Neural responses to perturbations in visual and auditory metronomes during sensorimotor synchronization. *Neuropsychologia*, *117*, 55–66. https://doi.org/10.1016/j.neuropsychologia.2018.05.013

Comstock, D. C., Hove, M. J., & Balasubramaniam, R. (2018). Sensorimotor synchronization with auditory and visual modalities: Behavioral and neural differences. *Frontiers in Computational Neuroscience*, *12*. https://doi.org/10.3389/fncom.2018.00053

Delorme, A., & Makeig, S. (2004). EEGLAB: An open source toolbox for analysis of single-trial EEG dynamics including independent component analysis. *Journal of Neuroscience Methods*, *134*(1), 9–21. https://doi.org/10.1016/j.jneumeth.2003.10.009

Destoky, F., Philippe, M., Bertels, J., Verhasselt, M., Coquelet, N., Vander Ghinst, M., Wens, V., De Tiège, X., & Bourguignon, M. (2019). Comparing the potential of MEG and EEG to uncover brain tracking of speech temporal envelope. *NeuroImage*, *184*, 201–213. https://doi.org/10.1016/j.neuroimage.2018.09.006

Engel, A. K., & Fries, P. (2010). Beta-band oscillations—Signalling the status quo? *Current Opinion in Neurobiology*, *20*(2), 156–165. https://doi.org/10.1016/j.conb.2010.02.015

Fitch, W. (2016). Dance, music, meter and groove: A forgotten partnership. *Frontiers in Human Neuroscience*, *10*, 64. https://doi.org/10.3389/fnhum.2016.00064

Fujioka, T., Ross, B., & Trainor, L. J. (2015). Beta-band oscillations represent auditory beat and its metrical hierarchy in perception and imagery. *Journal of Neuroscience*, *35*(45), 15187–15198. https://doi.org/10.1523/JNEUROSCI.2397-15.2015

Fujioka, T., Trainor, L., Large, E., & Ross, B. (2009). Beta and gamma rhythms in human auditory cortex during musical beat processing. *Annals of the New York Academy of Sciences*, *1169*(1), 89–92. https://doi.org/10.1111/j.1749-6632.2009.04779.x

Fujioka, T., Trainor, L. J., Large, E. W., & Ross, B. (2012). Internalized timing of isochronous sounds is represented in neuromagnetic beta oscillations. *Journal of Neuroscience*, *32*(5), 1791–1802. https://doi.org/10.1523/JNEUROSCI.4107-11.2012

Gan, L., Huang, Y., Zhou, L., Qian, C., & Wu, X. (2015). Synchronization to a bouncing ball with a realistic motion trajectory. *Scientific Reports*, *5*, 11974. https://doi.org/10.1038/srep11974

Gelman, A., & Stern, H. (2006). The difference between "significant" and "not significant" is not itself statistically significant. *The American Statistician*, *60*(4), 328–331. https://doi.org/10.1198/000313006X152649

Gordon, C. L., Cobb, P. R., & Balasubramaniam, R. (2018). Recruitment of the motor system during music listening: An ALE meta-analysis of fMRI data. *PLoS One*, *13*(11), e0207213. https://doi.org/10.1371/journal.pone.0207213

Grube, M., Cooper, F. E., Chinnery, P. F., & Griffiths, T. D. (2010). Dissociation of duration-based and beat-based auditory timing in cerebellar degeneration. *Proceedings of the National Academy of Sciences of the United States of America*, *107*(25), 11597–11601. https://doi.org/10.1073/pnas.0910473107

Grube, M., Lee, K. H., Griffiths, T. D., Barker, A. T., & Woodruff, P. W. (2010). Transcranial magnetic theta-burst stimulation of the human cerebellum distinguishes absolute, duration-based from relative, beat-based perception of subsecond time intervals. *Frontiers in Psychology*, *1*, 171. https://doi.org/10.3389/fpsyg.2010.00171

Haegens, S., & Golumbic, E. Z. (2018). Rhythmic facilitation of sensory processing: A critical review. *Neuroscience & Biobehavioral Reviews*, *86*, 150–165. https://doi.org/10.1016/j.neubiorev.2017.12.002

Hove, M. J., Fairhurst, M. T., Kotz, S. A., & Keller, P. E. (2013). Synchronizing with auditory and visual rhythms: An fMRI assessment of modality differences and modality appropriateness. *NeuroImage*, *67*, 313–321. https://doi.org/10.1016/j.neuroimage.2012.11.032

Hove, M. J., Iversen, J. R., Zhang, A., & Repp, B. H. (2013). Synchronization with competing visual and auditory rhythms: Bouncing ball meets metronome. *Psychological Research Psychologische Forschung*, *77*, 388–398. https://doi.org/10.1007/s00426-012-0441-0

Hove, M. J., Spivey, M. J., & Krumhansl, C. L. (2010). Compatibility of motion facilitates visuomotor synchronization. *Journal of Experimental Psychology: Human Perception and Performance*, *36*(6), 1525.

Iversen, J. R. (2016). In the beginning was the beat: Evolutionary origins of musical rhythm in humans. In R. Hartenberger (Ed.), *The Cambridge companion to percussion* (pp. 281–295). Cambridge University Press.

Iversen, J. R., & Balasubramaniam, R. (2016). Synchronization and temporal processing. *Current Opinion in Behavioral Sciences*, *8*, 175–180. https://doi.org/10.1016/j.cobeha.2016.02.027

Iversen, J. R., Patel, A. D., Nicodemus, B., & Emmorey, K. (2015). Synchronization to auditory and visual rhythms in hearing and deaf individuals. *Cognition*, *134*, 232–244. https://doi.org/10.1016/j.cognition.2014.10.018

Janata, P., Tomic, S. T., & Haberman, J. M. (2012). Sensorimotor coupling in music and the psychology of the groove. *Journal of Experimental Psychology: General*, *141*(1), 54. https://doi.org/10.1037/a0024208

Jäncke, L., Loose, R., Lutz, K., Specht, K., & Shah, N. J. (2000). Cortical activations during paced finger-tapping applying visual and auditory pacing stimuli. *Cognitive Brain Research*, *10*(1–2), 51–66. https://doi.org/10.1016/S0926-6410(00)00022-7

Jantzen, K. J., Steinberg, F. L., & Kelso, J. A. S. (2005). Functional MRI reveals the existence of modality and coordination-dependent timing networks. *NeuroImage*, *25*(4), 1031–1042. https://doi.org/10.1016/j.neuroimage.2004.12.029

Kaulmann, D., Hermsdörfer, J., & Johannsen, L. (2017). Disruption of right posterior parietal cortex by continuous Theta Burst Stimulation alters the control of body balance in quiet stance. *European Journal of Neuroscience*, *45*(5), 671–678. https://doi.org/10.1111/ejn.13522.

Kilavik, B. E., Zaepffel, M., Brovelli, A., MacKay, W. A., & Riehle, A. (2013). The ups and downs of beta oscillations in sensorimotor cortex. *Experimental Neurology*, *245*, 15–26. https://doi.org/10.1016/j.expneurol.2012.09.014

Kopell, N., Ermentrout, G. B., Whittington, M. A., & Traub, R. D. (2000). Gamma rhythms and beta rhythms have different synchronization properties. *Proceedings of the National Academy of Sciences of the United States of America*, *97*(4), 1867–1872. https://doi.org/10.1073/pnas.97.4.1867

Levitin, D. J., Grahn, J. A., & London, J. (2018). The psychology of music: Rhythm and movement. *Annual Review of Psychology*, *69*, 51–75. https://doi.org/10.1146/annurev-psych-122216-011740

Lorås, H., Sigmundsson, H., Talcott, J. B., Öhberg, F., & Stensdotter, A. K. (2012). Timing continuous or discontinuous movements across effectors specified by different pacing modalities and intervals. *Experimental Brain Research*, *220*(3–4), 335–347. https://doi.org/10.1007/s00221-012-3142-4

MATLAB (2019). *Version 9.6.0.1335978 (R2019b)*. Natick, MA: The MathWorks Inc.

Meijer, D., Te Woerd, E., & Praamstra, P. (2016). Timing of beta oscillatory synchronization and temporal prediction of upcoming stimuli. *NeuroImage*, *138*, 233–241. https://doi.org/10.1016/j.neuroimage.2016.05.071

Merchant, H., Grahn, J., Trainor, L., Rohrmeier, M., & Fitch, W. T. (2015). Finding the beat: A neural perspective across humans and non-human primates. *Philosophical Transactions of the Royal Society B: Biological Sciences*, *370*(1664). https://doi.org/10.1098/rstb.2014.0093

Merchant, H., Perez, O., Zarco, W., & Gamez, J. (2013). Interval tuning in the primate medial premotor cortex as a general timing mechanism. *Journal of Neuroscience*, *33*, 9082–9096.

Michalareas, G., Vezoli, J., Van Pelt, S., Schoffelen, J. M., Kennedy, H., & Fries, P. (2016). Alpha-beta and gamma rhythms subserve feedback and feedforward influences among human visual cortical areas. *Neuron*, *89*(2), 384–397. https://doi.org/10.1016/j.neuron.2015.12.018

Mullen, T. R., Kothe, C. A. E., Chi, Y. M., Ojeda, A., Kerth, T., Makeig, S., Jung, T.-P., & Cauwenberghs, G. (2015). Real-time neuroimaging and cognitive monitoring using wearable dry EEG. *IEEE Transactions on Biomedical Engineering*, *62*(11), 2553–2567. https://doi.org/10.1109/TBME.2015.2481482

Obleser, J., Eisner, F., & Kotz, S. A. (2008). Bilateral speech comprehension reflects differential sensitivity to spectral and temporal features. *Journal of Neuroscience*, *28*(32), 8116–8123. https://doi.org/10.1523/JNEUROSCI.1290-08.2008

Onton, J., Westerfield, M., Townsend, J., & Makeig, S. (2006). Imaging human EEG dynamics using independent component analysis. *Neuroscience & Biobehavioral Reviews*, *30*(6), 808–822. https://doi.org/10.1016/j.neubiorev.2006.06.007

Palmer, J. A., Kreutz-Delgado, K., & Makeig, S. (2012). *AMICA: An adaptive mixture of independent component analyzers with shared components*. Tech. Rep. Swartz Center for Computatonal Neursoscience, University of California San Diego.

Patel, A. D. (2006). Musical rhythm, linguistic rhythm, and human evolution. *Music Perception: An Interdisciplinary Journal*, *24*(1), 99–104. https://doi.org/10.1525/mp.2006.24.1.99

Patel, A. D., & Iversen, J. R. (2014). The evolutionary neuroscience of musical beat perception: The Action Simulation for Auditory Prediction (ASAP) hypothesis. *Frontiers in Systems Neuroscience*, *8*, 57. https://doi.org/10.3389/fnsys.2014.00057

Perception Research Systems. (2007). *Paradigm stimulus presentation*. Retrieved from http://www.paradigmexperiments.com

Piazza, C., Miyakoshi, M., Akalin-Acar, Z., Cantiani, C., Reni, G., Bianchi, A. M., & Makeig, S. (2016). *An automated function for identifying EEG independent components representing bilateral source activity*. In XIV Mediterranean conference on medical and biological engineering and computing 2016 (pp. 105–109), Springer, Cham.

Picazio, S., Veniero, D., Ponzo, V., Caltagirone, C., Gross, J., Thut, G., & Koch, G. (2014). Prefrontal control over motor cortex cycles at beta frequency during movement inhibition. *Current Biology*, *24*(24), 2940–2945. https://doi.org/10.1016/j.cub.2014.10.043

Pollok, B., Rothkegel, H., Schnitzler, A., Paulus, W., & Lang, N. (2008). The effect of rTMS over left and right dorsolateral premotor cortex on movement timing of either hand. *European Journal of Neuroscience*, *27*(3), 757–764. https://doi.org/10.1111/j.1460-9568.2008.06044.x.

Repp, B. H. (2003). Rate limits in sensorimotor synchronization with auditory and visual sequences: The synchronization threshold and the benefits and costs of interval subdivision. *Journal of Motor Behavior*, *35*, 355–370. https://doi.org/10.1080/00222890309603156

Repp, B. H. (2005). Sensorimotor synchronization: A review of the tapping literature. *Psychonomic Ulletin and Review*, *12*(6), 969–992. https://doi.org/10.3758/BF03206433.

Repp, B. H., & Penel, A. (2004). Rhythmic movement is attracted more strongly to auditory than to visual rhythms. *Psychological Research Psychologische Forschung*, *68*, 252–270. https://doi.org/10.1007/s00426-003-0143-8

Repp, B. H., & Su, Y. H. (2013). Sensorimotor synchronization: A review of recent research (2006–2012). *Psychonomic Bulletin & Review*, *20*, 403–452. https://doi.org/10.3758/s13423-012-0371-2

Ross, J. M., Iversen, J. R., & Balasubramaniam, R. (2016). Motor simulation theories of musical beat perception. *Neurocase*, *22*, 558–565. https://doi.org/10.1080/13554794.2016.1242756

Ross, J. M., Iversen, J. R., & Balasubramaniam, R. (2018). The role of posterior parietal cortex in beat-based timing perception: A continuous theta burst stimulation study. *Journal of Cognitive Neuroscience*, *30*, 634–643. https://doi.org/10.1162/jocn_a_01237

Ross, J. M., Warlaumont, A. S., Abney, D. H., Rigoli, L. M., & Balasubramaniam, R. (2016). Influence of musical groove on postural sway. *Journal of Experimental Psychology: Human Perception and Performance*, *42*(3), 308.

Saleh, M., Reimer, J., Penn, R., Ojakangas, C. L., & Hatsopoulos, N. G. (2010). Fast and slow oscillations in human primary motor cortex predict oncoming behaviorally relevant cues. *Neuron*, *65*(4), 461–471. https://doi.org/10.1016/j.neuron.2010.02.001

Sarnthein, J., Petsche, H., Rappelsberger, P., Shaw, G. L., & Von Stein, A. (1998). Synchronization between prefrontal and posterior association cortex during human working memory. *Proceedings of the National Academy of Sciences of the United States of America*, *95*(12), 7092–7096. https://doi.org/10.1073/pnas.95.12.7092

Schubotz, R. I., Friederici, A. D., & Von Cramon, D. Y. (2000). Time perception and motor timing: A common cortical and subcortical basis revealed by fMRI. *NeuroImage*, *11*(1), 1–12. https://doi.org/10.1006/nimg.1999.0514

Snyder, J. S., & Large, E. W. (2005). Gamma-band activity reflects the metric structure of rhythmic tone sequences. *Cognitive Brain Research*, *24*(1), 117–126. https://doi.org/10.1016/j.cogbrainres.2004.12.014

Varlet, M., Nozaradan, S., Trainor, L., & Keller, P. E. (2020). Dynamic modulation of beta band cortico-muscular coupling induced by audio-visual rhythms. *Cerebral Cortex Communications*, *1*(1), tgaa043. https://doi.org/10.1093/texcom/tgaa043

von Stein, A., & Sarnthein, J. (2000). Different frequencies for different scales of cortical integration: From local gamma to long range alpha/theta synchronization. *International Journal of Psychophysiology*, *38*, 301–313. https://doi.org/10.1016/S0167-8760(00)00172-0

Wiener, M., & Kanai, R. (2016). Frequency tuning for temporal perception and prediction. *Current Opinion in Behavioral Sciences*, *8*, 1–6. https://doi.org/10.1016/j.cobeha.2016.01.001

Wiener, M., Turkeltaub, P., & Coslett, H. B. (2010). The image of time: A voxel-wise meta-analysis. *NeuroImage*, *49*(2), 1728–1740. https://doi.org/10.1016/j.neuroimage.2009.09.064

Yadav, V., & Sainburg, R. L. (2014). Handedness can be explained by a serial hybrid control scheme. *Neuroscience*, *278*, 385–396. https://doi.org/10.1016/j.neuroscience.2014.08.026.

Zatorre, R. J., & Belin, P. (2001). Spectral and temporal processing in human auditory cortex. *Cerebral Cortex*, *11*(10), 946–953. https://doi.org/10.1093/cercor/11.10.946

Zatorre, R. J., Evans, A. C., Meyer, E., & Gjedde, A. (1992). Lateralization of phonetic and pitch discrimination in speech processing. *Science*, *256*(5058), 846–849.

Zhou, B., Yang, S., Mao, L., & Han, S. (2014). Visual feature processing in the early visual cortex affects duration perception. *Journal of Experimental Psychology: General*, *143*(5), 1893. https://doi.org/10.1037/a0037294

SUPPORTING INFORMATION

Additional supporting information may be found online in the Supporting Information section.

How to cite this article: Comstock DC, Ross JM, Balasubramaniam R. Modality-specific frequency band activity during neural entrainment to auditory and visual rhythms. *Eur J Neurosci*. 2021;00:1–21. https://doi.org/10.1111/ejn.15314